A COMPOSITE FRAME/JOINT SUPER ELEMENT FOR STRUCTURES STRENGTHENED BY EXTERNALLY BONDED STEEL/FRP PLATES

A THESIS SUBMITTED TO
THE GRADUATE SCHOOL OF NATURAL AND APPLIED SCIENCES
OF
THE MIDDLE EAST TECHNICAL UNIVERSITY

BY

YALÇIN KAYMAK

IN PARTIAL FULFILLMENT OF THE REQUIREMENTS FOR THE DEGREE OF
MASTER OF SCIENCE
IN
THE DEPARTMENT OF CIVIL ENGINEERING

MAY 2003

Approval of the Graduate School of Natural and Applied Sciences

_____

Prof. Dr. Tayfur Öztürk
Director

I certify that this thesis satisfies all the requirements as a thesis for the degree of Master of Science.

_____

Prof. Dr. Mustafa Tokyay
Head of Department

This is to certify that we have read this thesis and that in our opinion it is fully adequate, in scope and quality, as a thesis for the degree of Master of Science.

_____

Assoc. Prof. M. Ugur Polat
Supervisor

Examining Committee Members

Prof. Dr. Çetin Yilmaz _____

Prof. Dr. Mehmet Utku _____

Prof. Dr. S. Tanvir Wasti _____

Prof. Dr. Turgut Tokdemir _____

Assoc. Prof. M. Ugur Polat _____

ABSTRACT

A Composite Frame/Joint Super Element for Structures Strengthened by Externally Bonded Steel/FRP Plates

Kaymak, Yalçin
M.Sc., Department of Civil Engineering
Supervisor: Assoc. Prof. Dr. M. Ugur Polat

May 2003, 74 pages

A materially non-linear layered beam super element is developed for the analysis of RC beams and columns strengthened by externally bonded steel/FRP plates. The elasto-plastic behavior of RC member is incorporated by its internally generated or externally supplied moment-curvature diagram. The steel plate is assumed to be elasto-plastic and the FRP laminate is assumed to behave linearly elastic up to rupture. The thin epoxy layer between the RC member and the externally bonded lamina is simulated by a special interface element which allows for the changing failure modes from steel plate yielding/FRP plate rupture to separation of the bonded plates as a result of bond failure in the epoxy layer. An empirical failure criterion based on test results is used for the epoxy material of the interface.

The most critical aspect of such applications in real life frame structures is the anchorage conditions at the member ends and junctions. This has direct influence on the success and the effectiveness of the application. Therefore, a special corner piece anchorage element is also considered in the formulation of the joint super element, which establishes the fixity and continuity conditions at the member ends and the joints.

Keywords: nonlinear finite element method, super (macro) element, constraint equations, static condensation, frame element, interface element.

ÖZ

Çelik/Karbon Fiber Plakalar ile Güçlendirilmis Yapisal Sistemler için Bir Tabakali Kompozit Çerçeve/Dügüm Süper Elemani

Kaymak, Yalçin
Yüksek Lisans, Insaat Mühendisligi Bölümü
Tez Yöneticisi: Doç. Dr. Ugur Polat

Mayis 2003, 74 sayfa

Disaridan çelik veya karbon fiber plakalar yapistirilarak güçlendirilmis çerçeve tipi betonarme yapisal sistemlerin analiz ve tasarimi için malzeme davranisi olarak dogrusal olmayan bir kompozit kolon/kiris süper elemani gelistirilmistir. Betonarme elemanin elasto-plastik davranisi elemanin moment-egrilik iliskisi kullanilarak göz önüne alinmaktadir. Bu iliski kullanici tarafindan disaridan verilebilecegi gibi elemanin bilinen donati ve malzeme özellikleri göz önüne alinarak otomatik olarak da hesaplanabilmektedir. Çelik plakalarin elasto-plastik, FRP plakalar ise kopma noktasina kadar dogrusal elastik davrandigi var sayilmaktadir. Çelik veya karbon fiber plaka ile betonarme eleman yüzeyi arasindaki ince yapiskan tabaka ise özel bir arayüz sonlu elemani ile modellenmektedir. Arayüz elemaninda literatürde mevcut test sonuçlarina dayanan ampirik bir kirilma kriteri kullanilmakta olup bu arayüz elemani yapistirilan çelik plakanin akmasi veya karbon fiber tabakanin kopmasindan baslayarak tabakalarin beton yüzeyden ayrismasina kadar degisen göçme mekanizmalarini modelleyebilmektedir.

Bu tür yapisal güçlendirme yaklasiminin pratikteki uygulamalarinda en kritik unsur yapistirilan plakalarin eleman uçlarindaki veya birlesimlerdeki ankraj sartlaridir. Bu ankraj durumu uygulamanin basarisini ve etkinligini dogrudan etkilemektedir. Bu nedenle özel bir köse baglanti ve ankraj elemani da dügüm süper elemani formülasyonuna dahil edilmistir. Bu sayede eleman uçlarindaki ve

birlesimlerdeki ankraj ve süreklilik sartlari süper elemanin davranisina yansitilabilmektedir.

Anahtar Sözcükler: dogrusal olmayan sonlu elemanlar yöntemi, süper (makro) eleman, kisit denklemleri, statik yogunlastirma, çerçeve elemani, arayüz elemani.

To My Supervisor Dr. M. Ugur Polat

ACKNOWLEDGMENTS

I would like to express my sincere thanks to my thesis supervisor, Assoc. Prof. M. Ugur Polat for his great guidance and encouragement throughout this research effort. I have learnt many things about engineering, the way of thinking, personal relationships and life from him. I consider myself fortunate to study with such an exceptional instructor.

I would like to express my deepest gratitude to Prof. Dr. Yalçin Mengi for the courses I took through my M.Sc. study. He is a marvelous instructor having strong work ethics and excellent research skills.

I am also grateful to my friends especially Raci Bayer, Tugsan Çelebi, Sükrü Güzey, Celal Soyarslan, Sinan Akarsu, Hüsnü Dal, Seval Pinarbasi, Ufuk Yazgan, Farahnaz Altidjafarbay and all others for their friendly help and continued support.

Finally, I would like to offer my special thanks to my family for their encouragement, unyielding patience and endless support throughout my life. Without their support, I could never have achieved this level of success.

TABLE OF CONTENTS

LIST OF TABLES

LIST OF FIGURES

LIST OF SYMBOLS

L	Length of frame element
a,b	Rigid zone lengths of frame element
N,$\underline{N}$	Shape functions, and shape function vector
$\underline{\varepsilon}$	Strain tensor for frame element in Equation (2.2)
ε,?	Axial strain and curvature in a section of frame element
$\underline{B}$	Strain-displacement matrix for frame element in Equation (2.2)
$\underline{s}$	Stress tensor for frame element in Equation (2.3)
$\underline{D}$	Constitutive matrix for stress-strain relation of frame element
$\underline{K},\underline{R},\underline{U}$	Stiffness matrix, displacement and response vectors of FE's
EA, EI	Axial rigidity and bending Rigidities of frame element
N,M	Axial load and bending moment
$\underline{J}$	Jacobian matrix
$\underline{T}$	Rigid zone transformation matrix in Equation (2.8)
$\underline{I}$	Identity matrix
L_t,L_b	Top and bottom face length of interface element in Figure 2.4
Ls	Top face starting offset length of interface element in Figure 2.4
H	Thickness of interface element in global Y direction in Figure 2.4
w	Thickness of interface element in global Z direction
x,y	Global coordinates of interface element in Figure 2.4
r,s	Local coordinates of interface element in Figure 2.4
$\underline{X},\underline{U}$	Nodal coordinates and displacements of interface element
$\underline{\tilde{B}}$, $\underline{B}$	Strain-displacement matrix for interface element in Equation (2.14)
τ_{cr}	Separation shear stress of interface element in Figure 2.6
γ_{cr}	Separation shear strain of interface element in Figure 2.6
G	Shear modulus
E	Elasticity modulus
$\underline{D}$	Constitutive matrix for stress-strain relation of interface element
$\underline{T}$,$\underline{T}_B$,$\underline{T}_T$	Constraint transformation matrices of interface element
$\underline{T}$(L,y)	Pure beam transformation for interface element in Equation (2.21)
$\underline{T}$(a,b)	Rigid zone transformation matrix in Equation (2.21)
$\underline{T}$(L,a,y)	Rigid body constraint transformation matrix in Equation (2.23)
$\Delta\underline{U}$,$\Delta\underline{F}$	Incremental displacement and force vectors

${}^{t}\underline{U}$, ${}^{t+\Delta t}\underline{U}$	Displacement vector at time t and t+Δt
m,n	Number of integration points in r- and s-directions
α_{ij}	Integration point weight
$\underline{K}_{mm}, \underline{K}_{ss}, \underline{K}_{ms}$	Partitions of super element stifness matrix in Equation (2.26)
$\Delta\underline{U}_m, \Delta\underline{U}_s$	Partitions of super element incremental displacement vector
$\Delta\underline{F}_m, \Delta\underline{F}_s$	Partitions of super element incremental force vector
$\underline{K}_{cc}$	Condensed super element stiffness matrix
$\Delta\underline{F}_c$	Condensed super element incremental force vector
P,F	Point loads
θ	Tip rotation in Equation (3.1)
Δ	Tip deflection in Equation (3.1)
N_1, N_2, N_3	Number of super element subdivisions
A_s, A_s'	Tension and compression steel areas
σ_{xy}, σ_{yy}	Shear and normal stresses
b,h	Width and height of RC section in Figure B.1
A_{st}, A_{sb}	Top and bottom steel area of RC section in Figure B.1
M_{cr}, M_y, M_u	Cracking, Yield and Ultimate moments of RC section
$\phi_{cr}, \phi_y, \phi_u$	Cracking, Yield and Ultimate curvatures of RC section
A_s	Tension steel area
c,d	Neutal axis depth and tension steel depth
β_1	Rectangular stress block constant
f_y, ε_y	Tension steel yield strength and strain
?	Steel ratio of RC section
n	Modulus of elasticity ratio of steel to concrete
E_c, E_s	Concrete and steel modulus of elasticity
I_g	Moment of inertia of concrete section
f_c, f_r	Concrete compressive strength and rupture modulus

CHAPTER 1

INTRODUCTION

1.1 Statement of the Problem

Most of the reinforced concrete (RC) frame structures in Turkey lack strength and stiffness to resist seismic loads. Structures may required to be strengthened not only for increasing earthquake resistance but also for increasing safety, change in service, correcting design and production errors, explosion resistance, unforeseen loads, design code changes, and retrofitting. There are various approaches to strengthening or retrofitting of the RC frame structures. One alternative is to replace the infill and partition walls with load carrying shear (structural) walls. Another way is to increase the load carrying capacity of beams and columns of the structure by jacketing. A very practical way of increasing the flexural strength and stiffness of RC frames is to use externally bonded steel or fiber reinforced polymer (FRP) plates on the faces of its beams and columns. The use of FRP is considered as the state-of-the-art strengthening and retrofitting technique because the method has some superior characteristics over others. The basic advantage is that the increase in the element cross-sectional dimensions and the weight is very negligible. Moreover, the application of FRP is very easy and practical.

Many of the finite element (FE) programs perform linear analysis only. However, the behavior of RC frame structures highly nonlinear. For an effective and economical design, it is evident that one has to perform the analysis considering nonlinearities. However, most of the commercial FE package programs perform linear analysis only. A few more advanced FE packages give the opportunity of using concentrated nonlinear springs to model the nonlinearities to a limited extent. Still, this is

inadequate as the plastifications are spread over a region and are not concentrated. Most of the engineers use moment reduction factors by intuition to account for the redistribution of stresses and perform capacity design at the joints.

In order to get satisfactory results from a FE analysis, the density of the finite element mesh must be high enough and the size of the elements must be small enough. Although the computer technology develops incredibly fast, nonlinear analysis of large structures still requires very high capacities and takes a lot of computational time.

The approach taken in this study to the analysis of such structures is to use nonlinear frame and interface elements to model the members and joints of the strengthened frame structures. The idea of developing finite element based frame and joint super elements for the nonlinear analysis of two-dimensional frame structures sounds very attractive. This approach is expected to decrease not only the required time for solution, but also the required computer capacity for large structural systems. It is anticipated that this, in turn, helps the engineer work on more sophisticated and realistic mathematical models of such structures.

Until recently, the quality of software was being measured by its memory management and the speed of execution. Today's software has to satisfy some additional requirements as well. Existing literature insists that the important software quality parameters are correctness, robustness, extensibility, reusability, compatibility, efficiency, functionality, ease of use, and ease of maintenance. C++ programming language is highly convenient for this purpose since it can improve significantly most of these factors.

1.2 Literature Survey

Recently, there have been enormous developments related to materials, methods, and techniques for structural engineering. Composite materials are innovative products of the so-called advanced engineering era. One of today's state-of-the-art techniques for structural upgrading is the use of FRP composites. These plastics are currently viewed by structural engineers as new and highly promising materials in the construction industry. Typical properties of FRP material are shown in Table 1.1.

Table 1.1 Typical properties of FRP composites, E.E. Gdoutos, et al. [4]

Material		Elastic Modulus (GPa)	Tensile Strength (MPa)	Ultimate Tensile strain (%)
Carbon				
	High strength	215-235	3800-4800	> 1.4
	Ultra high strength	215-235	3800-6200	> 1.5
	High modulus	350-500	> 3100	> 0.5
	Ultra high modulus	500-700	> 2400	> 0.2
Glass				
	E	70	1850-2700	> 4.5
	S	85-90	3500-4800	> 5.4
Aramid				
	Low modulus	70-80	3500-4100	> 2.5
	High modulus	110-125	3500-4100	> 1.6

RC frame elements, such as beams and columns, may be strengthened in flexure by the use of steel/FRP plates epoxy-bonded to their tension zones. This technique is simple and effective as far as both the cost and the mechanical performance are concerned. The use of steel plates suffers from several disadvantages: corrosion of plates resulting in bond deterioration; difficulty in manipulating heavy plates in tight construction sites; need for scaffolding; and limitation in available plate lengths for flexural strengthening of long girders, resulting in need for joints. Replacing the steel plates with FRP strips provides satisfactory solutions to these problems. FRP composites suffer from certain disadvantages too, which are not to be neglected by the engineers. In contrast to steel, which behaves in an elasto-plastic manner, the FRP composites, in general, are linear elastic up to failure. The failure occurs without any significant yielding or plastic deformation-induced ductility but at large strains. Comparative idealized stress-strain curves of concrete, steel and FRP material for mathematical modeling are show in Figure 1.1 and the shear-slip models for the interface material are shown in Figure 1.2. The cost of FRP materials on a weight basis is several times higher than that for steel though when cost comparison is made on a strength basis, they become less unfavorable. Moreover, some fibers, e.g., carbon or aramid, are anisotropic, resulting in incompatible thermal expansion coefficients between composites and concrete. Finally, their exposure to high temperatures, e.g., in case of a fire, may cause premature degradation and collapse because some epoxy resins start softening at about 80°C. FRP material should not be thought of blindly as a replacement for steel or other materials in structural intervention applications. E.E. Gdoutos, K. Pilakoutas, and C.A. Rodopoulos [4].

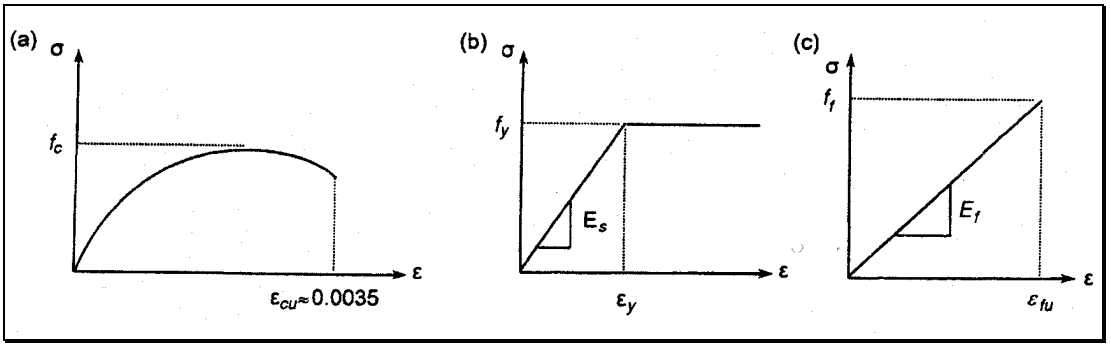

Figure 1.1 Idealized stress-strain curves for (a) concrete in compression; (b) steel in tension or compression; (c) FRP in tension, E.E. Gdoutos et al. [4]

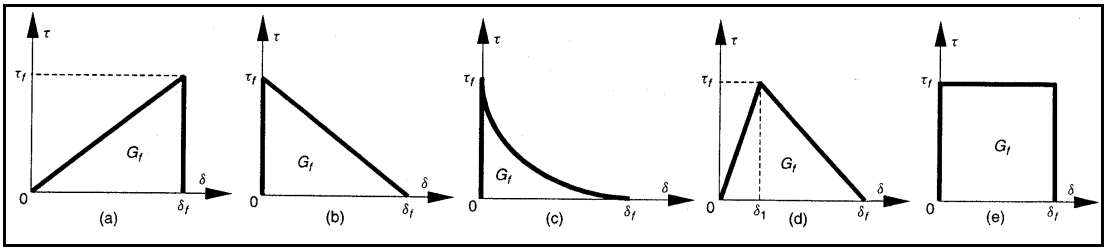

Figure 1.2 Shear-slip models for plate to concrete bonded joints, J.G. Teng et al. [3]

Understanding the failure mechanism and failure criteria of FRP is very important for the designer. Most commonly observed failure modes in composites are delamination and debonding which are the separations of the individual plies. Failure modes are classified into seven main categories as shown in Figure 1.3, by J.G. Teng, et al [3]. Collectively, failure modes (d) and (e) are referred to as plate-end debonding failures, while failure modes (f) and (g) are referred to as intermediate crack-induced interfacial debonding failures.

J.G. Teng, et al [3] describe 12 failure models in detail. They categorize these models in three groups as (a) shear-capacity-based models, (b) concrete tooth models, and (c) interfacial stress-based models. All of the models are represented by using a consistent notation and in a form that best facilitates comparisons between them.

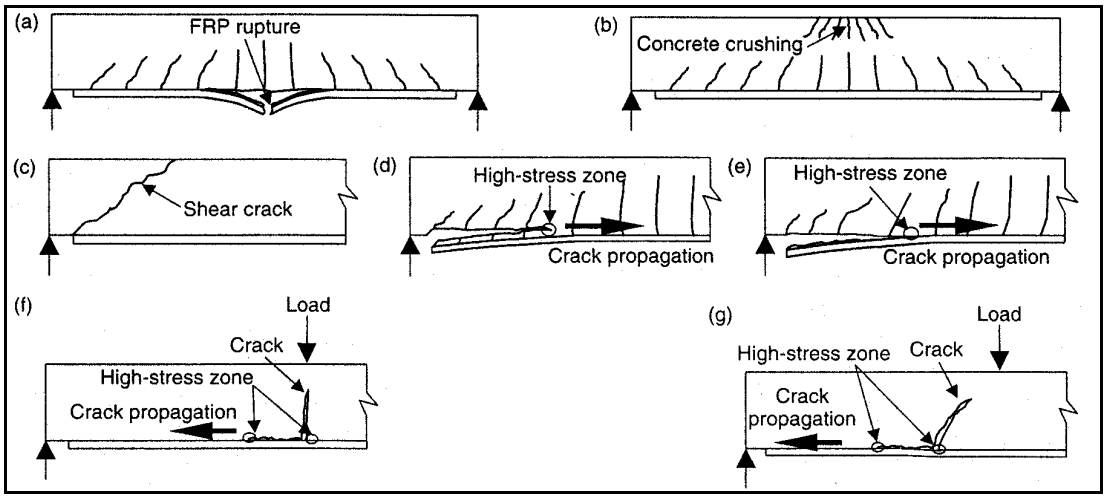

Figure 1.3 Failure modes of FRP-plated RC beams: (a) FRP rupture; (b) crushing of compressive concrete; (c) shear failure; (d) concrete cover separation; (e) plate-end interfacial debonding; (f) intermediate flexural crack-induced interfacial debonding; (g) intermediate flexural shear crack-induced interfacial debonding, J.G. Teng et al. [3]

1.2.1 Experimental Studies

In 2001, D. Duthinh, and M. Starnes, [5] have tested seven concrete beams reinforced internally with varying amounts of steel and externally with carbon FRP laminates applied after the concrete had cracked under service loads. They measured strains along the beam depth for computation of the beam curvature in the constant moment region. Experiment results were shown that FRP is very effective for flexural strengthening. Clamping or wrapping of the ends of the laminate enhances the capacity of adhesively bonded FRP anchorage. They also discussed the design equations for anchorage, allowable stress, ductility, and amount of reinforcement.

In 2001, L. De Lorenzis, B. Miller, A. Nanni [6] prepared flexural test specimens to address some of the factors expected to affect the bond, namely, the bonded length, concrete strength, number of plies (stiffness), sheet width and, to a limited extent, surface preparation. They presented and discussed the results. They used a shear lag approach, along with a simple shear model for the evaluation of the slip modulus to model the strain distribution at moderate load levels. Finally, they presented expressions of the peeling load and the effective bond length. They proposed a design equation to calculate the effective FRP ultimate strain to be used in design to account for the bond-controlled failure.

In 2001, A.J. Lamanna, L.C. Bank, and D.W. Scott [7] presented a feasibility of an alternative method of attaching FRP strips to RC beams. The method utilizes off-the-shelf powder-actuated fasteners to attach pultruded FRP strip to the concrete. They tested small sized beams strengthened with this method, and compared the results with conventional bonding methods and to the results from control beams. Small-sized beams strengthened using powder-actuated fasteners attained 65 to 70% of the increase in capacity of the beams strengthened using conventional bond method. However, the fastening method is extremely rapid and the failure modes were more ductile than those strengthened by the conventional bonding method

1.2.2 Analytical Studies

In 2001, J.F. Chen and J.G. Teng [8] presented a review of current anchorage strength models for both FRP-to-concrete and steel-to-concrete bonded joints under shear. Then, they assessed these models with experimental data collected from the literature, revealing the deficiencies of all existing models. Finally, they proposed a new simple and rational model based on an existing fracture mechanics analysis and experimental observations. This new model not only matches experimental observations of bond strength closely, but also correctly predicts the effective bond length. The new model is thus suitable for practical application in the design of FRP-to-concrete as well as steel-to-concrete bonded joints.

In 2002, S.T. Smith and J.G. Teng [9, 10] represented a comprehensive review of existing plate debonding strength models. The most commonly reported failure occurs at or near the plate end, by either separation of the concrete cover or interfacial debonding of the FRP plate from the RC beam. The two papers are concerned with the 12 strength models for such plate end debonding failures. Each model is summarised and classified into one of the three categories based on the approach taken, and its theorerical basis clarified.

In 2001, Y. Qiu, M.A. Crisfield, G. Alfano [11] described a simple corotational one-dimensional interface element formulation for the simulation of delamination with buckling. They took into account the geometrical and material nonlinearity. They made detailed comparisons with experimental results for such a problem.

In 1999, G. Li, P. Lee-Sullivan, and R.W. Thring [12] performed a geometrically nonlinear, two-dimensional (2D) FE analysis to determine the stress and strain distributions across the adhesive bond thickness of composite single-lap joints. They presented the results of simulations for 0.13 and 0.26 mm bond thickness. They found good agreement with the experimental results by using 2-element and 6-element mesh schemes for the thinner bond layer. Further mesh refinement using a 10-element for the thicker bond has shown that both the tensile peel and shear stresses at the bond free edges change significantly across the adhesive thickness. Both stresses became increasingly higher with distance from the centerline and peak near but not along the adherent-adhesive interface.

In 2001, P.C. Pandey, and S. Narasimhan [13] presented a three-dimensional (3D) viscoplastic analysis of adhesively bonded single lap joint considering material and geometric nonlinearity. The constitutive relations used for the adhesive is developed using a pressure dependent (modified) von Mises yield function and Ramberg-Osgood idealization. They modeled adherents and adhesive layers by using 20-node solid elements. They carried out materially and geometrically nonlinear FE analysis on several joint configurations.

In 1998, S.W. Hansen [14] developed a dynamic model for a multilayered laminated plate which consists of 2n plate layers and 2n – 1 adhesive layers. The layers (both plate and adhesive layers) are assumed to be homogeneous, transversely isotropic and perfectly bonded to one another. In the initial modeling, the Reissner-Mindlin theory of shear deformable plates is applied to each layer, resulting in a high-order plate theory in which the shear motions of layers are completely independent. Simpler lower-order models are obtained from the initial model from asymptotic limits based upon the assumptions that (i) the adhesive layers are very thin, (ii) the elastic modulii of the adhesive layers are small as compared to those of the plate layers, (iii) the shear stiffnesses of the plate layers are very large.

In 2001, V. Colotti and G. Spadea [15] presented a truss model capable of describing the ultimate behavior of externally bonded RC beams. The effectiveness of the proposed approach is validated by comparing the obtained numerical results with some experimental data that is available in the literature.

In order to overcome the layered beam problems S.K. Kassegne and J.N. Reddy [16] developed a two dimensional stiffener element for laminated composite shells and

plates based on the Layerwise Theory of Reddy for composite laminates. The element has a displacement field compatible with that of a layerwise plate or cylindrical shell element and can be efficiently employed as a stiffener for such structural elements. The element can also be used as a stand-alone curved or straight beam element. A finite element model of the theory is developed and used to validate the accuracy and stability of this element for the bending, buckling and natural vibration analysis of stand-alone curved and straight composite laminated beam.

Recently, R. Tanov, A. Tabiei [17] developed a new homogenization procedure for FE analysis of sandwich shells. To the authors' knowledge all present FE approaches to sandwich structures are incorporated into the FE formulation on the element formulation level. Unlike other formulations, the present approach works on the constitutive level. A homogenization of the sandwich shell is performed at each call of the corresponding constitutive subroutine. Thus, the sandwich nature of the problem is hidden from the main FE program. As a consequence, there is no need to develop a new shell element formulation, instead all available homogeneous shell elements in the utilized FE code can be used for the analysis of sandwich shells. This would provide versatility of the FE analysis and potentials to trade off between the level of accuracy and computational efficiency by using more accurate or simpler shell elements. Furthermore, the sandwich homogenization procedure can be easily coupled with a composite homogenization model to enable analysis of sandwich shells with composite faces. To validate the present approach and check its accuracy, efficiency and overall performance, it is implemented in a FE package and combined with existing first-order shear deformable shell elements for homogeneous materials. Results are obtained and herein presented for problems previously investigated experimentally and by different theoretical and numerical techniques. The presented results show good agreement with published results from far more complicated and computationally intensive analyses, which build confidence in the approach and motivate its future elaboration and development.

S. Singh and I.K. Partridge [18] studied the mechanisms and the extent of toughening. Unidirectional laminates were tested in mode-I, mode-II and in mixed mode by means of the modified NASA mixed-mode bending rig. They found significant increases in delamination resistance in all modes of loading when they placed 50 and 200 μm thick layers of the resin in the central crack path of the laminates. The fracture data were fitted to simple failure criterion and related to the

predicted plastic zone sizes. Fractographic examination documents the gradual change in the micro-mechanisms of failure as the imposed loading mode changes. The crack path is observed to oscillate between the two ply boundaries, via the resin-rich layer, raising questions as to the micromechanical interpretation of the fracture data.

In 1998, H. Luo and S. Hanagud [19] present a new model for composite beams with through-width delaminations. They took in to account shear effect, end rotary inertia terms, as well as bending-extension coupling in the governing equations of vibration. Nonlinear interaction, due to piecewise linear spring models between the delaminated sublaminates, is also included. Based on this model, eigen-solutions for vibrations of intact and delaminated beams are found analytically. Dynamic behavior predicted by this model is then compared with previously reported experimental results. They found better agreements with the experimental results. They explained discrepancies among previously proposed models without difficulty.

In 2001, F. Shen, K.H. Lee, and T .E. Tay [20] presented a computational model for the prediction of delamination growth in laminated composites. In the analysis of post-buckled delaminations, an important parameter is the distribution of the local strain-energy release rate along the delamination front. They made a study using virtual crack closure technique for three-dimensional finite-element models of circular delaminations embedded in woven and non-woven composite laminates. The delamination is embedded at different depths along the thickness direction of the laminates. They discussed the issue of symmetry boundary conditions. They found that fiber orientation of the plies in the delaminated part play an important role in the distribution of the local strain-energy release rate. This implies that the popular use of quarter models in order to save computational effort is unjustified and will lead to erroneous results. They made comparison with experimental results and predicted growth of the delamination front with fatigue cycling. They also described a methodology for the prediction of delamination areas and directions using evolution criteria derived from test coupon data. They found that evolution criteria based on components of the strain-energy release rate predict the rate of delamination growth much better than evolution criteria based on the total strain energy release rate.

In 1998, N. El-Abbasi and S.A. Meguid [21] presented a new 7-parameter shell model for thick shel1 applications. The model accounts explicitly for the thickness

change in the shell, as well as the normal stress and strain through the shell thickness. They account for large deformations by using the second Piola-Kirchhoff stress and the Green-Lagrange strain tensors. They used an assumed transverse shear strain interpolation in order to avoid shear locking. They developed two new interpolation schemes for the shell director in order to avoid thickness locking. These interpolations are implemented and their consistent linearization is derived. They developed guidelines for neglecting some of the quadratic terms in the consistent stiffness matrix to minimize computational time. They tested the thick shell element performance in order to show that the higher order terms result in improved accuracy. They also demonstrated that for thin shells, there is no significant deterioration in accuracy, as compared with traditional 5-parameter shell elements.

In 2000, O.T. Thomsen [22] presented a high-order plate theory formulation, which includes the through-thickness flexibility, and which inherently includes a description of the global response as well as the local responses of the individual layers of an arbitrary multi-layer structural plate assembly. The features of the high-order multi-layer plate theory are demonstrated through analysis of the elastic response of a CFRP/honeycomb-cored sandwich panel with symmetric exterior ply drops. The chosen example involves a 7-Iayer sandwich plate assembly that changes to a 3-layer assembly at the position of the ply-drops.

1.3 Objective

Recently, there have been many researches on the subject of structural strengthening by the use of FRP material. Nonetheless, there are a limited number of analytical tools to perform the nonlinear analysis of this type of frame structures. Most of the commercial FE packages are not designed to perform such analysis although the FE method is very suitable for performing the job. The FE model generation, preparing realistic models and post processing of the output with the available packages are very time consuming, difficult and, consequently, not practical for the engineers.

The load carrying capacity of the member in structures strengthened by externally bonded steel/FRP plates is determined mainly by the separation of steel or FRP plates from the RC member face and at the joints. The separation usually starts in

the RC face of the epoxy layer at highly stressed regions. Nonlinear characteristics of the moment-curvature relations of RC members, stress-strain relation of steel plates and the brittle behavior of FRP and bonding epoxy restrict the use of linear FE packages for the investigation of failure modes and the overall response.

The joints of frame structures are subjected to high shear forces and bending moments. Hence, it is very important to maintain their integrity. The use of a special corner piece element in such applications is found to be very essential for the anchorage. They are also very effective in increasing the strength and the stiffness of the joints besides maintaining their integrity. In addition, these pieces form convenient locations for mounting brace elements.

The main objective of this study is to formulate nonlinear frame and joint super (macro) elements, which will facilitate the analysis of frame structures, strengthened with externally bonded steel/FRP plates. Super elements are defined and represented by their coupling nodes just like an ordinary FE but they automatically generate their internal domain nodes. Hence, the structural stiffness matrix will be rather small compared to regular FE model of the same structure. Therefore, the required computer capacity and the solution time are expected to be small even for large structural systems.

The frame and the joint super elements are capable of determining the failure mechanisms. Therefore, the separation of plates from the RC face or at the end anchorage points near the joints and breaking off or yielding of steel/FRP plates in the span can be modeled by means of these super elements.

CHAPTER 2

ELEMENT FORMULATIONS AND IMPLEMENTATION

2.1 Introduction

There are some serious difficulties encountered by the engineers in the finite element analysis of frame structural systems strengthened by externally bonded steel/FRP plates. The generation of the mathematical model and the processing of the analysis results are of major concerns for such structures even by today's powerful computers and sophisticated general purpose FE programs. The preparation of the mathematical model is a time consuming process because the mesh of the model contains many frame and interface elements whose DOF's are related by constraint equations. Secondly, there is a memory and speed problem even with today's powerful computers. This is caused by the excessive number of active degrees of freedom in the finite element model. The severity of the problem increases very rapidly with the increasing size and complexity of the structural system. Finally, there are serious difficulties in the post-processing phase of the analysis results due to its large volume. This difficulty also increases with the increasing size and complexity of the model.

Finite element modelling of a given strengthened frame structure is a rather boring and time consuming process demanding a lot of patience and energy on the part of the engineer. The process also creates a very conducive environment for making mistakes. Basic difficulties encountered in various stages of the process can be summarized as follows.

- Discretization and calculation of the nodal point coordinates to be used in defining the finite element mesh of the frame structure.
- Meshing the structure based on the nodal points assigned and defining the element connectivity in terms of these nodal points.
- Defining the external excitations acting on the structure with reference to the nodal points, which requires some preliminary calculations by the engineer before the analysis is carried out.

All of these problems decrease the efficiency and the speed of the structural analysis. The work in this study is focused on formulating and implementing a nonlinear finite element analysis program for strengthened frame structures. The program contains frame element, interface element, frame super element and joint super element in its element library. A super element is a complex type of element, which includes a number of finite elements used in structural modelling. It is also termed as a substructure. Substructuring is a well-known technique, which is frequently used in structural engineering to reduce the size of the problem to be solved. Super elements are believed to relieve substantially the difficulties stated above.

2.2 Nonlinear Frame Element

A nonlinear frame element is developed in order to model the displacement and stress variation in the RC beam and steel/FRP plates. Frame element is formulated based on the Euler-Bernoulli beam assumptions given by Cook [1]. A typical frame element and its degrees of freedom (DOF's), its rigid end offset lengths "a" and "b", and its flexible length "L" are shown in Figure 2.1.

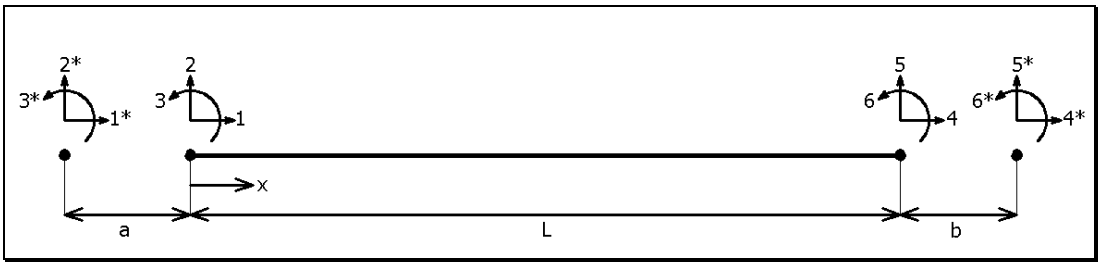

Figure 2.1 Frame element dimensions and DOF's

Frame element shape functions corresponding to DOF's shown in Figure 2.1 are given in Equation (2.1). For axial deformation u, linear interpolation functions N_1 and N_4 are used. For transverse deformation v, the Hermitian interpolation functions N_2, N_3, N_5 and N_6 are used. Rotations θ are obtained from the derivative of the transverse deformation v.

$$\underline{N}(x)=\begin{bmatrix} N_1(x)\\ N_2(x)\\ N_3(x)\\ N_4(x)\\ N_5(x)\\ N_6(x)\end{bmatrix}=\begin{bmatrix} 1-\frac{x}{L}\\ 1-\frac{3x^2}{L^2}+\frac{2x^3}{L^3}\\ x-\frac{2x^2}{L}+\frac{x^3}{L^2}\\ \frac{x}{L}\\ \frac{3x^2}{L^2}-\frac{2x^3}{L^3}\\ -\frac{x^2}{L}+\frac{x^3}{L^2}\end{bmatrix} \qquad (2.1)$$

The variation of shape functions, N_1 and N_4 for axial deformation u over a flexible length L of the frame element is shown in Figure 2.2.

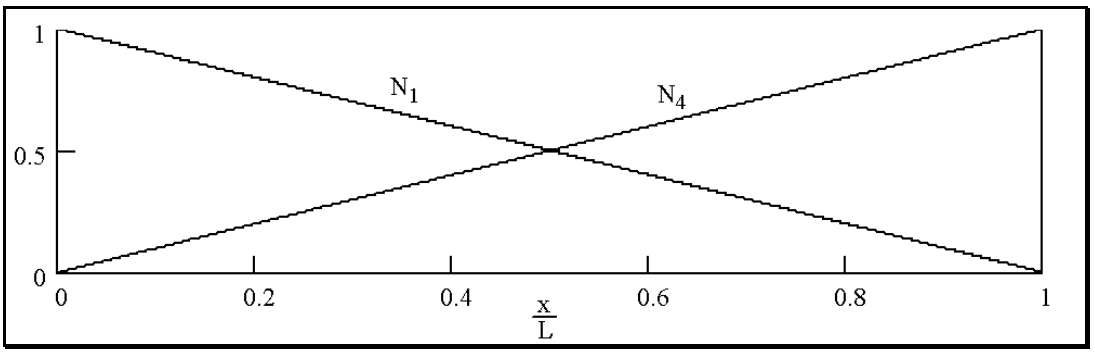

Figure 2.2 Shape functions for frame element axial deformation

The variation of shape functions, N_2, N_3, N_5, and N_6 for transverse deformation v over the flexible length L of the frame element is shown in Figure 2.3.

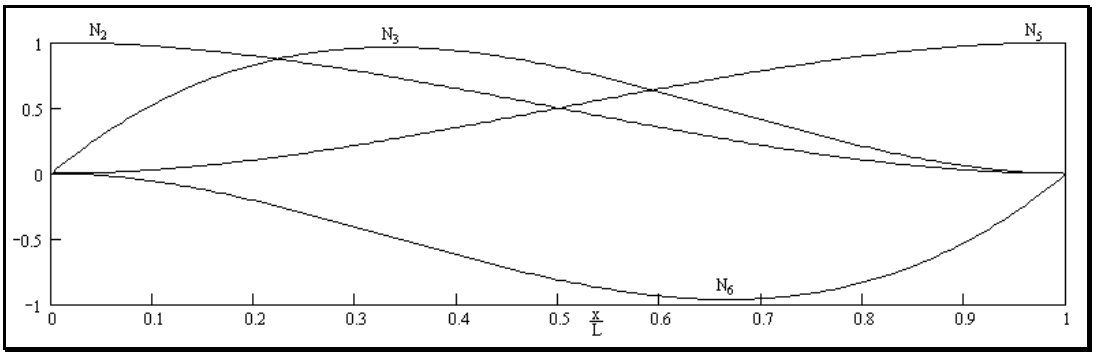

Figure 2.3 Shape functions for frame element transverse deformation

Strain displacement matrix B relates the displacement vector U to strain vector ?. Expressions for strain vector ? and the strain-displacement matrix B are given in Equation (2.2). In these equations, ε is the axial strain, ? is the curvature and x is the distance from starting node along the flexible length L of the frame element.

$$\underline{\varepsilon} = \begin{bmatrix} \varepsilon \\ \kappa \end{bmatrix} = \underline{B} \cdot \underline{U}$$

$$\underline{B} = \begin{bmatrix} -\frac{1}{L} & 0 & 0 & \frac{1}{L} & 0 & 0 \\ 0 & -\frac{6}{L^2}+\frac{12x}{L^3} & -\frac{4}{L}+\frac{6x}{L^2} & 0 & \frac{6}{L^2}-\frac{12x}{L^3} & -\frac{2}{L}+\frac{6x}{L^2} \end{bmatrix} \qquad (2.2)$$

Constitutive matrix D relates the strain vector ? to stress vector s. It is calculated by using the moment-curvature relation of the frame element section and the uniaxial stress-strain relation of the material. The expressions for the stress vector s and the constitutive matrix D are given in Equation (2.3). In these equations, N is the axial force, M is the bending moment, EA is the axial rigidity and EI is the flexural rigidity at a given section of the frame element.

$$\underline{\sigma} = \begin{bmatrix} N \\ M \end{bmatrix} = \underline{D} \cdot \underline{\varepsilon}$$

$$\underline{D} = \begin{bmatrix} EA & 0 \\ 0 & EI \end{bmatrix} \qquad (2.3)$$

Nonlinear frame element will be part of the frame and joint super elements. There are two possible orientations for the frame element in the local coordinates of super elements. It can either be horizontal or vertical. To provide efficiency, instead

of multiplying by a rotation matrix, only row and column operations are performed on the stiffness matrix $\underline{K}$ and the response vector $\underline{R}$ for vertical elements. There may also be rigid end offsets. For this, the rigid end zone transformation matrix $\underline{T}$, given in Equation (2.8), is used in order to modify the element stiffness matrix and the response vector.

2.2.1 Frame Element Tangential Stiffness Matrix

The frame element tangential stiffness matrix $\underline{K}$ can be computed by the integral given in Equation (2.4). The stiffness matrix is a function of the element properties, EI, EA and L. Bending rigidity EI and axial rigidity EA are considered to be constant over the element. EI is taken from the slope of the moment-curvature diagram at a given curvature (the average curvature in the frame element). EA is obtained by multiplying modulus of elasticity E which is taken from the slope of the stress-strain diagram at a given axial strain level ? by the cross-sectional area A which is considered to be constant over the frame element. Under the assumptions stated, the integral expression in first line of Equation (2.4) can be evaluated exactly to obtain the tangential stiffness matrix $\underline{K}$. Once the element properties EA, EI, and L are known, its tangential stiffness matrix can easily be formed. The expression for the frame element tangential stiffness matrix in local coordinate system is given in last line of Equation (2.4).

$$\underline{K} = \int_0^L \underline{B}^T \cdot \underline{D} \cdot \underline{B}\, dx$$

$$\underline{K} = \int_{-1}^{+1} \underline{B}^T \cdot \underline{D} \cdot \underline{B} \cdot \left|\underline{J}\right| ds$$

$$\underline{K} = \sum_{i=1}^{n} {}^{i}\underline{B}^T \cdot {}^{i}\underline{D} \cdot {}^{i}\underline{B} \cdot \left|{}^{i}\underline{J}\right| \cdot \alpha_i$$

$$\underline{K} = \begin{bmatrix} \frac{EA}{L} & 0 & 0 & -\frac{EA}{L} & 0 & 0 \\ 0 & \frac{12EI}{L^3} & \frac{6EI}{L^2} & 0 & -\frac{12EI}{L^3} & \frac{6EI}{L^2} \\ 0 & \frac{6EI}{L^2} & \frac{4EI}{L} & 0 & -\frac{6EI}{L^2} & \frac{2EI}{L} \\ -\frac{EA}{L} & 0 & 0 & \frac{EA}{L} & 0 & 0 \\ 0 & -\frac{12EI}{L^3} & -\frac{6EI}{L^2} & 0 & \frac{12EI}{L^3} & -\frac{6EI}{L^2} \\ 0 & \frac{6EI}{L^2} & \frac{2EI}{L} & 0 & -\frac{6EI}{L^2} & \frac{4EI}{L} \end{bmatrix} \qquad (2.4)$$

2.2.2 Frame Element Response Vector

Computation of the response is the vital part in a nonlinear analysis. In this nonlinear frame element formulation, small deformation theory is used and geometric nonlinearities are not taken into account. Therefore, the axial and the flexural effects are considered to be uncoupled and only material nonlinearities are taken into account. Given a displacement vector $\underline{U}$, which is considered to be small, the response vector $\underline{R}$ is computed by the following integral.

$$\underline{R} = \int_0^L \underline{B}^T \cdot \underline{\sigma}\, dx$$
$$\underline{R} = \int_{-1}^{+1} \underline{B}^T \cdot \underline{\sigma} \cdot \left|\underline{J}\right| ds \qquad (2.5)$$
$$\underline{R} = \sum_{i=1}^{n} {}^i\underline{B}^T \cdot {}^i\underline{\sigma} \cdot \left|{}^i\underline{J}\right| \cdot \alpha_i$$

The integral given in Equation (2.5) is evaluated numerically by Gauss quadrature. Strain-displacement matrix $\underline{B}$ and stress vector $\underline{s}$ are obtained at integration points as given in Equation (2.6).

$$x = \frac{L}{2} + \frac{L}{2} \cdot s \qquad \Rightarrow \qquad \left|\underline{J}\right| = \left|\frac{dx}{ds}\right| = \frac{L}{2}$$
$${}^i\underline{B} = \underline{B}(x_i) \qquad (2.6)$$
$${}^i\underline{\sigma} = {}^i\underline{D} \cdot {}^i\underline{B} \cdot \underline{U} \qquad (i = 1,2)$$

2.2.3 Rigid End Zone Transformation Matrix

The rigid end zone transformation matrix $\underline{T}$ is used to account for the rigid end zones of the frame element. The displacement vector $\underline{U}^*$, the tangential stiffness matrix $\underline{K}$, and the response vector $\underline{R}$ are transformed as given in Equation (2.7).

$$\underline{U} = \underline{T} \cdot \underline{U}^*$$
$$\underline{K}^* = \underline{T}^T \cdot \underline{K} \cdot \underline{T} \qquad (2.7)$$
$$\underline{F}^* = \underline{T}^T \cdot \underline{F}$$

Given the frame element rigid end zone lengths “a” and “b”, one can easily obtain the rigid end zone transformation matrix by using Equation (2.8).

$$\underline{T} = \begin{bmatrix} 1 & 0 & 0 & 0 & 0 & 0 \\ 0 & 1 & a & 0 & 0 & 0 \\ 0 & 0 & 1 & 0 & 0 & 0 \\ 0 & 0 & 0 & 1 & 0 & 0 \\ 0 & 0 & 0 & 0 & 1 & -b \\ 0 & 0 & 0 & 0 & 0 & 1 \end{bmatrix} \tag{2.8}$$

Note that when the rigid end zone lengths “a” and “b” are zero, the transformation matrix $\underline{T}$ would become an identity matrix, $\underline{I}$. and no transformation is realized. For computational efficiency the matrix operations given in Equation (2.7) are performed using the variables “a” and “b”, only.

2.3 Nonlinear Interface Element

A nonlinear interface element is developed in order to model the displacement, strain and stress variation in the adhesive layer between RC frame member and the steel/FRP plates. The formulation of the interface element is based on the isoparametric element formulation given in Bathe [2]. A typical interface element and its components are shown in Figure 2.4 in global coordinate system. In order to define the nodal coordinates of the interface elements, the element height H, the bottom and the top face lengths “Lb” and “Lt”, and the starting node offset length “Ls” must be given.

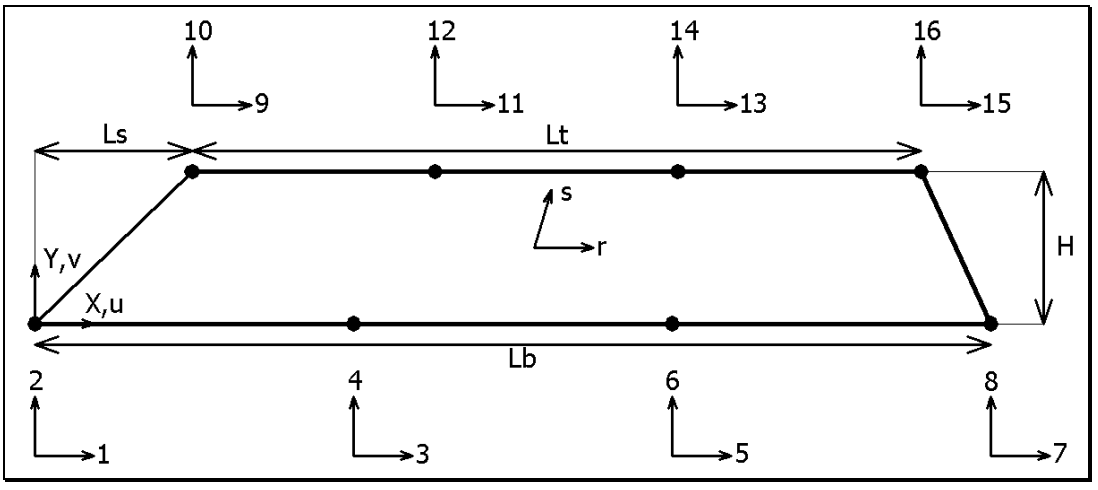

Figure 2.4 Interface element dimensions and DOF’s

Parent interface element in local coordinate system is shown in Figure 2.5. Polynomial shape functions are derived on the basis of the parent element. The expressions for the shape functions corresponding to DOF's shown in Figure 2.4 and their derivatives are given in Equation (2.9)

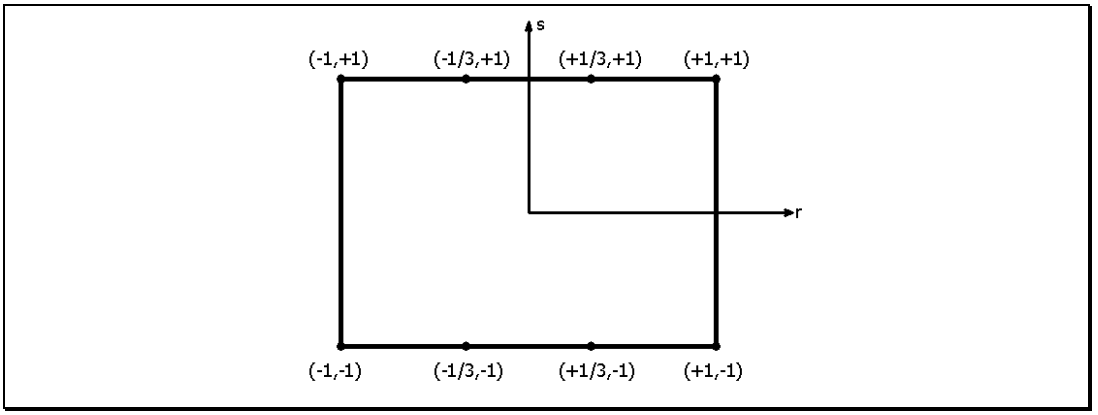

Figure 2.5 Parent interface element

$$\underline{N}(r,s)=\frac{1}{32}\begin{bmatrix}-(1-9r^2)(1-r)(1-s)\\ 9(1-3r)(1-r^2)(1-s)\\ 9(1+3r)(1-r^2)(1-s)\\ -(1-9r^2)(1+r)(1-s)\\ -(1-9r^2)(1-r)(1+s)\\ 9(1-3r)(1-r^2)(1+s)\\ 9(1+3r)(1-r^2)(1+s)\\ -(1-9r^2)(1+r)(1+s)\end{bmatrix}$$

$$\frac{\partial \underline{N}}{\partial r}=\frac{1}{32}\begin{bmatrix}(1+18r-27r^2)(1-s)\\ (-3-2r+9r^2)(1-s)\\ (3-2r-9r^2)(1-s)\\ (-1+18r+27r^2)(1-s)\\ (1+18r-27r^2)(1+s)\\ (-3-2r+9r^2)(1+s)\\ (3-2r-9r^2)(1+s)\\ (-1+18r+27r^2)(1+s)\end{bmatrix}\qquad \frac{\partial \underline{N}}{\partial s}=\frac{1}{32}\begin{bmatrix}(1-9r^2)(1-r)\\ -9(1-3r)(1-r^2)\\ -9(1+3r)(1-r^2)\\ (1-9r^2)(1+r)\\ -(1-9r^2)(1-r)\\ 9(1-3r)(1-r^2)\\ 9(1+3r)(1-r^2)\\ -(1-9r^2)(1+r)\end{bmatrix} \tag{2.9}$$

The interface element must be accurate for large aspect ratios, which is $\max(L_b,L_t)/H$, in order to provide the computational efficiency. For large aspect ratios, displacement, strain and stress vary widely r-direction whereas the variation of the same variables along s-direction is very minor and can accurately be estimated by linear interpolation functions. Thereby, the required number of

nodes and integration points along r-direction is more than that in s-direction. Hence, there are four nodes along r-direction to provide a cubic displacement field in r-direction and two nodes along s-direction, which provide a linear displacement field in s-direction. Moreover, the number of integration points in r-direction is three and in s-direction is two.

In order to avoid numerical instability, the aspect ratio must be limited. The patch tests and eigenvalue analyses performed on the stiffness matrix of interface element have shown that the interface element behavior and the numerical results are satisfactory for aspect ratios up to 200. However, in the implementation of the program the maximum allowable aspect ratio is set to 100 to be on the safe side.

Nodal coordinates of the interface element with respect to global coordinate system are given by the matrix $\underline{\tilde{X}}$. Nodal displacements of the interface element with respect to the global coordinate system are represented in matrix form by $\underline{\tilde{U}}$, and in vector form by $\underline{U}$. In the formulation and the implementation, both forms are used for the sake of efficiency and readability of the program developed. In Equation (2.10), the subscripts B and T refers to the bottom and the top face of the interface element, respectively. Numbers 1 to 4 represents the position of the node from left side of the interface element.

$$\underline{\tilde{X}} = \begin{bmatrix} x_{B1} & x_{B2} & x_{B3} & x_{B4} & x_{T1} & x_{T2} & x_{T3} & x_{T4} \\ y_{B1} & y_{B2} & y_{B3} & y_{B4} & y_{T1} & y_{T2} & y_{T3} & y_{T4} \end{bmatrix}^T$$

$$\underline{\tilde{U}} = \begin{bmatrix} u_{B1} & u_{B2} & u_{B3} & u_{B4} & u_{T1} & u_{T2} & u_{T3} & u_{T4} \\ v_{B1} & v_{B2} & v_{B3} & v_{B4} & v_{T1} & v_{T2} & v_{T3} & v_{T4} \end{bmatrix}^T \qquad (2.10)$$

$$\underline{U} = [u_{B1} \quad v_{B1} \quad u_{B2} \quad v_{B2} \quad u_{B3} \quad v_{B3} \quad u_{B4} \quad v_{B4} \quad \cdots \quad \cdots \; u_{T1} \quad v_{T1} \quad u_{T2} \quad v_{T2} \quad u_{T3} \quad v_{T3} \quad u_{T4} \quad v_{T4}]^T$$

Given the local coordinates (r,s) of a material point, the corresponding global coordinates (x,y) and the displacements (u,v) with respect to the global coordinate system are determined by using the nodal coordinate matrix $\underline{\tilde{X}}$, the nodal displacement matrix $\underline{\tilde{U}}$, and the shape functions $\underline{N}$, as given in Equation (2.11).

$$\underline{x}(r,s)=\begin{bmatrix}x(r,s)\\ y(r,s)\end{bmatrix}=\underset{\sim}{\underline{X}}^{T}\cdot\underline{N}(r,s)$$

$$\underline{u}(r,s)=\begin{bmatrix}u(r,s)\\ v(r,s)\end{bmatrix}=\underset{\sim}{\underline{U}}^{T}\cdot\underline{N}(r,s) \qquad (2.11)$$

Transpose of the Jacobian matrix $\underline{J}^T$ relates the shape function derivatives with respect to global coordinates (x,y) to shape function derivatives with respect to local coordinates (r,s) as given in Equation (2.12). This relation is inverted to find the shape function derivatives with respect global coordinates (x,y) at a given material point in local coordinates (r,s).

$$\begin{bmatrix}\dfrac{\partial\,\underline{N}(r,s)}{\partial r}\\ \dfrac{\partial\,\underline{N}(r,s)}{\partial s}\end{bmatrix}=\underline{J}^{T}\cdot\begin{bmatrix}\dfrac{\partial\,\underline{N}(x,y)}{\partial x}\\ \dfrac{\partial\,\underline{N}(x,y)}{\partial y}\end{bmatrix}$$

$$\begin{bmatrix}\dfrac{\partial\,\underline{N}(x,y)}{\partial x}\\ \dfrac{\partial\,\underline{N}(x,y)}{\partial y}\end{bmatrix}=\underline{J}^{-T}\cdot\begin{bmatrix}\dfrac{\partial\,\underline{N}(r,s)}{\partial r}\\ \dfrac{\partial\,\underline{N}(r,s)}{\partial s}\end{bmatrix} \qquad (2.12)$$

Definition of the Jacobian matrix $\underline{J}$ for the coordinate transformation from local coordinates (r,s) to global coordinates (x,y) is given in Equation (2.13).

$$\underline{J}(r,s)=\begin{bmatrix}j_{11} & j_{12}\\ j_{21} & j_{22}\end{bmatrix}=\begin{bmatrix}\dfrac{\partial x(r,s)}{\partial r} & \dfrac{\partial x(r,s)}{\partial s}\\ \dfrac{\partial y(r,s)}{\partial r} & \dfrac{\partial y(r,s)}{\partial s}\end{bmatrix}$$

$$\underline{J}^{-T}=\frac{1}{j_{11}\cdot j_{22}-j_{21}\cdot j_{12}}\cdot\begin{bmatrix}j_{22} & -j_{21}\\ -j_{12} & j_{11}\end{bmatrix} \qquad (2.13)$$

There are two forms of the strain-displacement matrix; $\underset{\sim}{\underline{B}}$ and $\underline{B}$. The first form of the strain-displacement matrix $\underset{\sim}{\underline{B}}$ relates the displacement matrix $\underset{\sim}{\underline{U}}$ to the strain matrix $\underset{\sim}{\underline{\varepsilon}}$. This form is more convenient to be used in the response calculations. Likewise, the second form of the strain-displacement matrix $\underline{B}$ relates the displacement vector $\underline{U}$ to the strain vector $\underline{\varepsilon}$. This form is more convenient to be used in the stiffness calculations together with the constitutive matrix $\underline{D}$. The explicit forms of $\underset{\sim}{\underline{B}}$ and $\underline{B}$ are given in Equation (2.14).

$$\tilde{\underline{B}}(r,s)=\begin{bmatrix} \frac{\partial \underline{N}_1}{\partial x} & \frac{\partial \underline{N}_2}{\partial x} & \frac{\partial \underline{N}_3}{\partial x} & \frac{\partial \underline{N}_4}{\partial x} & \frac{\partial \underline{N}_5}{\partial x} & \frac{\partial \underline{N}_6}{\partial x} & \frac{\partial \underline{N}_7}{\partial x} & \frac{\partial \underline{N}_8}{\partial x} \\ \frac{\partial \underline{N}_1}{\partial y} & \frac{\partial \underline{N}_2}{\partial y} & \frac{\partial \underline{N}_3}{\partial y} & \frac{\partial \underline{N}_4}{\partial y} & \frac{\partial \underline{N}_5}{\partial y} & \frac{\partial \underline{N}_6}{\partial y} & \frac{\partial \underline{N}_7}{\partial y} & \frac{\partial \underline{N}_8}{\partial y} \end{bmatrix}$$

$$\underline{B}(r,s)=\begin{bmatrix} \frac{\partial \underline{N}_1}{\partial x} & 0 & \frac{\partial \underline{N}_2}{\partial x} & 0 & \frac{\partial \underline{N}_3}{\partial x} & 0 & \frac{\partial \underline{N}_4}{\partial x} & 0 \\ 0 & \frac{\partial \underline{N}_1}{\partial y} & 0 & \frac{\partial \underline{N}_2}{\partial y} & 0 & \frac{\partial \underline{N}_3}{\partial y} & 0 & \frac{\partial \underline{N}_4}{\partial y} \\ \frac{\partial \underline{N}_1}{\partial y} & \frac{\partial \underline{N}_1}{\partial x} & \frac{\partial \underline{N}_2}{\partial y} & \frac{\partial \underline{N}_2}{\partial x} & \frac{\partial \underline{N}_3}{\partial y} & \frac{\partial \underline{N}_3}{\partial x} & \frac{\partial \underline{N}_4}{\partial y} & \frac{\partial \underline{N}_4}{\partial x} \end{bmatrix} \ldots$$

$$\ldots \begin{bmatrix} \frac{\partial \underline{N}_5}{\partial x} & 0 & \frac{\partial \underline{N}_6}{\partial x} & 0 & \frac{\partial \underline{N}_7}{\partial x} & 0 & \frac{\partial \underline{N}_8}{\partial x} & 0 \\ 0 & \frac{\partial \underline{N}_5}{\partial y} & 0 & \frac{\partial \underline{N}_6}{\partial y} & 0 & \frac{\partial \underline{N}_7}{\partial y} & 0 & \frac{\partial \underline{N}_8}{\partial y} \\ \frac{\partial \underline{N}_5}{\partial y} & \frac{\partial \underline{N}_5}{\partial x} & \frac{\partial \underline{N}_6}{\partial y} & \frac{\partial \underline{N}_6}{\partial x} & \frac{\partial \underline{N}_7}{\partial y} & \frac{\partial \underline{N}_7}{\partial x} & \frac{\partial \underline{N}_8}{\partial y} & \frac{\partial \underline{N}_8}{\partial x} \end{bmatrix} \qquad (2.14)$$

An empirical material model is used for the interface element such that separation of steel/FRP plates from RC frame member can be modeled mathematically in the interface element. However, in reality, the separation occurs between the adhesive layer and the RC frame member. There are a number of bond strength models many of which are explained in Teng [3]. The current interface element formulation is based on a bond strength model, which is linear elastic up to a critical shear strain γ_{cr}. The model is graphically represented in Figure 2.6.

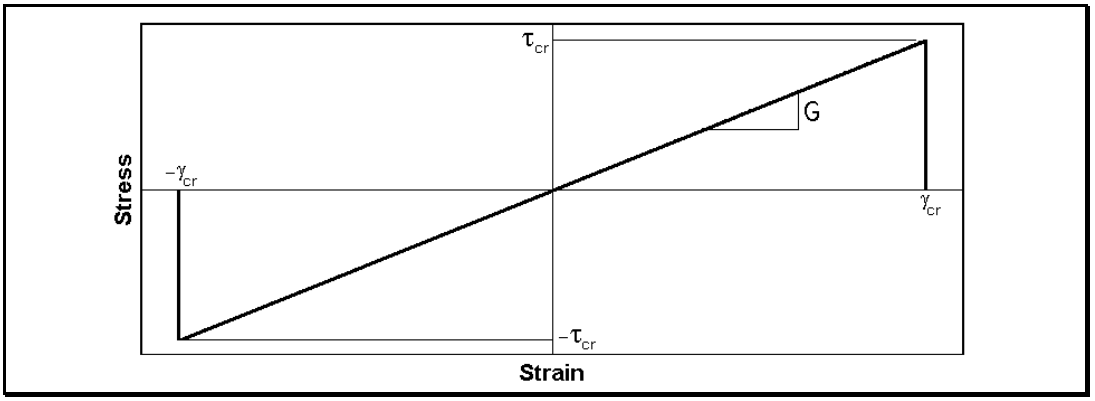

Figure 2.6 Interface element material model

The modulus of elasticity E is related to the shear modulus G which is determined through the material model. Details are given in Equation (2.15).

$$G = \frac{t_{cr}}{?_{cr}} \qquad E = 2 \cdot (1 + ?) \cdot G \tag{2.15}$$

The constitutive matrix $\underline{D}$ relates the strain vector $\underline{?}$ to stress vector $\underline{s}$ as given in the Equation (2.16). It is calculated by using the modulus of elasticity E and the Poisson's ratio ?.

$$\underline{s}(r,s) = \underline{D} \cdot \underline{e}(r,s)$$
$$\underline{D} = \frac{E}{1 - ?^2} \cdot \begin{bmatrix} 1 & ? & 0 \\ ? & 1 & 0 \\ 0 & 0 & \frac{1-?}{2} \end{bmatrix} \tag{2.16}$$

When the average shear stress over the element exceeds the critical shear stress τ_{cr}, the interface element is assumed to be inactive. The average shear stress over the element is computed from the response vector. Horizontal components of the response vector are summed up to give the total shear force on the element. The average shear stress is computed as the total shear force divided by element area.

The current interface element is part of the frame and joint super elements. There are two possible orientations for the interface element in the local coordinates of super elements. It can either be horizontal or vertical. In order to increase the computational efficiency, the stiffness matrix $\underline{K}$ and the response vector $\underline{R}$ for the vertical elements are obtained through some row and column operations from the corresponding horizontal element instead of the pre- and/or post-multiplying by the rotation matrix.

2.3.1 Interface Element Constraint Equations

The displacement, stiffness and the response quantities of the interface element must be compatible with those of the frame elements and rigid corner pieces. Beam and rigid body constraint equations (or transformation matrix $\underline{T}$) are used to transform the displacement vector $\underline{U}$, the stiffness matrix $\underline{K}$, and the response vector $\underline{R}$ to provide this compatibility. In order not to deal with zero parts, the transformation matrix can be partitioned into two parts as $\underline{T}_B$ for the bottom face and $\underline{T}_T$ for the top face, as given in Equation (2.17).

$$
\begin{aligned}
\underline{T} &= \begin{bmatrix} \underline{T}_B & \underline{0} \\ \underline{0} & \underline{T}_T \end{bmatrix} \\
\underline{T} \cdot \underline{U}^* &= \begin{bmatrix} \underline{T}_B & \underline{0} \\ \underline{0} & \underline{T}_T \end{bmatrix} \cdot \begin{bmatrix} \underline{U}_B^* \\ \underline{U}_T^* \end{bmatrix} = \begin{bmatrix} \underline{T}_B \cdot \underline{U}_B^* \\ \underline{T}_T \cdot \underline{U}_T^* \end{bmatrix} \\
\underline{T}^T \cdot \underline{K} \cdot \underline{T} &= \begin{bmatrix} \underline{T}_B & \underline{0} \\ \underline{0} & \underline{T}_T \end{bmatrix}^T \cdot \begin{bmatrix} \underline{K}_{BB} & \underline{K}_{BT} \\ \underline{K}_{TB} & \underline{K}_{TT} \end{bmatrix} \cdot \begin{bmatrix} \underline{T}_B & \underline{0} \\ \underline{0} & \underline{T}_T \end{bmatrix} = \begin{bmatrix} \underline{T}_B^T \cdot \underline{K}_{BB} \cdot \underline{T}_B & \underline{T}_B^T \cdot \underline{K}_{BT} \cdot \underline{T}_T \\ \underline{T}_T^T \cdot \underline{K}_{TB} \cdot \underline{T}_B & \underline{T}_T^T \cdot \underline{K}_{TT} \cdot \underline{T}_T \end{bmatrix} \\
\underline{T}^T \cdot \underline{R} &= \begin{bmatrix} \underline{T}_B & \underline{0} \\ \underline{0} & \underline{T}_T \end{bmatrix}^T \cdot \begin{bmatrix} \underline{R}_B \\ \underline{R}_T \end{bmatrix} = \begin{bmatrix} \underline{T}_B^T \cdot \underline{R}_B \\ \underline{T}_T^T \cdot \underline{R}_T \end{bmatrix}
\end{aligned}
\qquad (2.17)
$$

These parts may either represent the beam constraints or the rigid body constraints. Components of transformation matrices can be determined by using the relation between the constrained DOF's and the interface element DOF's. Geometrical dimensions and DOF numbering of a typical interface element is shown in Figure 2.7.

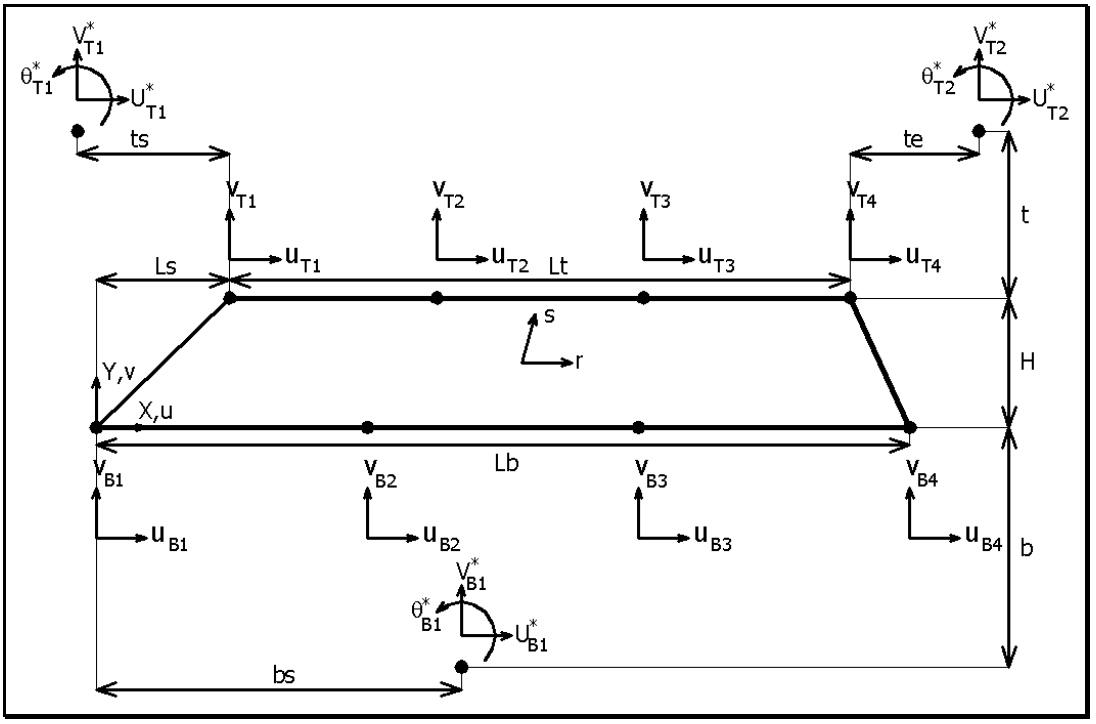

Figure 2.7 Geometric dimensions and DOF numbering of an interface element

The interface element shown in Figure 2.7 has rigid body constraints at the bottom face and beam constraints at the top face. Given the geometric dimensions,

transformation matrices $\underline{T}_B$ for bottom face and $\underline{T}_T$ for top face can be computed. Details of the computation are given in the following two sections.

2.3.1.1 Beam Constraint Equations

Consider a beam with flexible length L and rigid zone lengths a and b as shown in Figure 2.8. Let $\underline{U}$ be the vector of displacement components at the two ends of the flexible portion of the beam and $\underline{U}^*$ be the vector of displacement components at the ends of the whole beam including the rigid zones. The displacement vectors $\underline{U}$ and $\underline{U}^*$are related to each other by the rigid end zone transformation matrix $\underline{T}(a,b)$ as given in Equation (2.18).

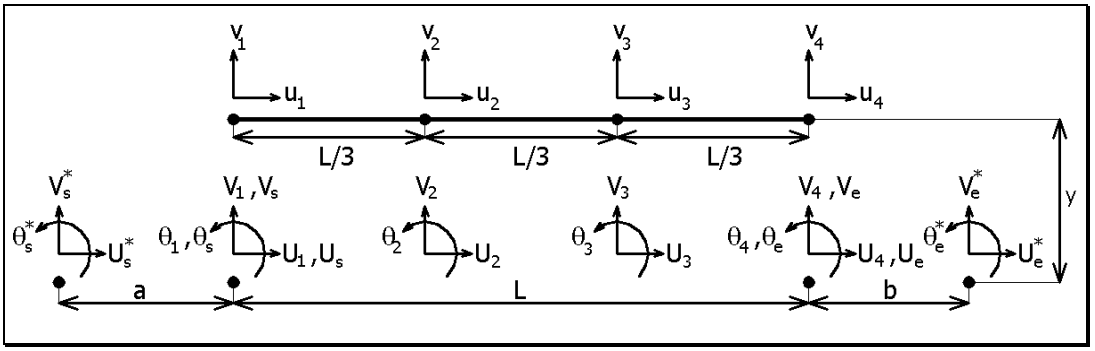

Figure 2.8 Beam constraints for interface element

$$\begin{aligned} \underline{U}^* &= \begin{bmatrix} U_s^* & V_s^* & \theta_s^* & U_e^* & V_e^* & \theta_e^* \end{bmatrix}^T \\ \underline{U} &= \begin{bmatrix} U_s & V_s & \theta_s & U_e & V_e & \theta_e \end{bmatrix}^T \\ \underline{U} &= \underline{T}(a,b) \cdot \underline{U}^* \end{aligned} \qquad (2.18)$$

The expression for the rigid end zone transformation matrix $\underline{T}(a,b)$ is the same as the one given for the frame element in Section (2.1) in Equation (2.9) above. The displacement fields u, v, and θ over the flexible portion of the frame element are given in Equation (2.19) in which N_1 to N_6 are the beam element shape functions given in Equation (2.1).

$$\begin{aligned} u(x) &= U_s \cdot N_1 + U_e \cdot N_4 \\ v(x) &= V_s \cdot N_2 + \theta_s \cdot N_3 + V_e \cdot N_5 + \theta_e \cdot N_6 \\ \theta(x) &= \frac{dv}{dx} = V_s \cdot \frac{dN_2}{dx} + \theta_s \cdot \frac{dN_3}{dx} + V_e \cdot \frac{dN_5}{dx} + \theta_e \cdot \frac{dN_6}{dx} \end{aligned} \qquad (2.19)$$

The flexible portion of the frame element is divided into three equal segments to establish its compatibility to the interface element. The axial, the transverse and the rotational displacements at the newly generated internal nodes along center line can easily be determined by Equation (2.20).

$$
\begin{aligned}
U_2 &= u\left(\frac{L}{3}\right) = \frac{2U_s}{3} + \frac{U_e}{3} \\
V_2 &= v\left(\frac{L}{3}\right) = \frac{20V_s}{27} + \frac{4L\theta_s}{27} + \frac{7V_e}{27} - \frac{2L\theta_e}{27} \\
\theta_2 &= \theta\left(\frac{L}{3}\right) = -\frac{4V_s}{3L} + \frac{4V_e}{3L} - \frac{\theta_e}{3} \\
U_3 &= u\left(\frac{2L}{3}\right) = \frac{U_s}{3} + \frac{2U_e}{3} \\
V_3 &= v\left(\frac{2L}{3}\right) = \frac{7V_s}{27} + \frac{2L\theta_s}{27} + \frac{20V_e}{27} - \frac{4L\theta_e}{27} \\
\theta_3 &= \theta\left(\frac{2L}{3}\right) = -\frac{4V_s}{3L} - \frac{\theta_s}{3} + \frac{4V_e}{3L}
\end{aligned}
\tag{2.20}
$$

The nodal DOF's along the top and the bottom face of the interface element are related to the adjacent beam element through Euler-Bernoulli assumption. All constraint equations related to the beam constraints are combined in the transformation matrix $\underline{T}(L,a,b,y)$. See Equation (2.21)

$$
\begin{aligned}
&u_i = U_i - y\cdot\theta_i \quad (i = 1,2,3, \text{ and } 4) \\
&v_i = V_i \\
&\underline{T}(L,y) = \begin{bmatrix}
1 & 0 & -y & 0 & 0 & 0 \\
0 & 1 & 0 & 0 & 0 & 0 \\
\frac{2}{3} & \frac{4y}{3L} & 0 & \frac{1}{3} & -\frac{4y}{3L} & \frac{y}{3} \\
0 & \frac{20}{27} & \frac{4L}{27} & 0 & \frac{7}{27} & -\frac{2L}{27} \\
\frac{1}{3} & \frac{4y}{3L} & \frac{y}{3} & \frac{2}{3} & -\frac{4y}{3L} & 0 \\
0 & \frac{7}{27} & \frac{2L}{27} & 0 & \frac{20}{27} & -\frac{4L}{27} \\
0 & 0 & 0 & 1 & 0 & -y \\
0 & 0 & 0 & 0 & 1 & 0
\end{bmatrix} \\
&\underline{T}(L,a,b,y) = \underline{T}(L,y)\cdot\underline{T}(a,b)
\end{aligned}
\tag{2.21}
$$

Transformation matrix $\underline{T}(L,y)$ which is given in Equation (2.21) represents the pure beam constraint equations of the flexible part of the frame elements. It should be noted that the parameter y in Equation (2.21) is to be set to "b" and "–t" for the

bottom and the top faces of the interface element, respectively. The parameters “b” and “t” are the distances between the beams centerline and the adjacent face of the interface element as shown in Figure 2.7. These constraint equations are used for defining the interface element boundary node DOF’s in terms the frame element nodal DOF’s

2.3.1.2 Rigid Body Constraint Equations

Consider a node with DOF’s, U^*, V^*, and θ^* as shown in Figure 2.9. Assume that the nodes on the top or bottom face of the interface element are connected to this node with rigid links.

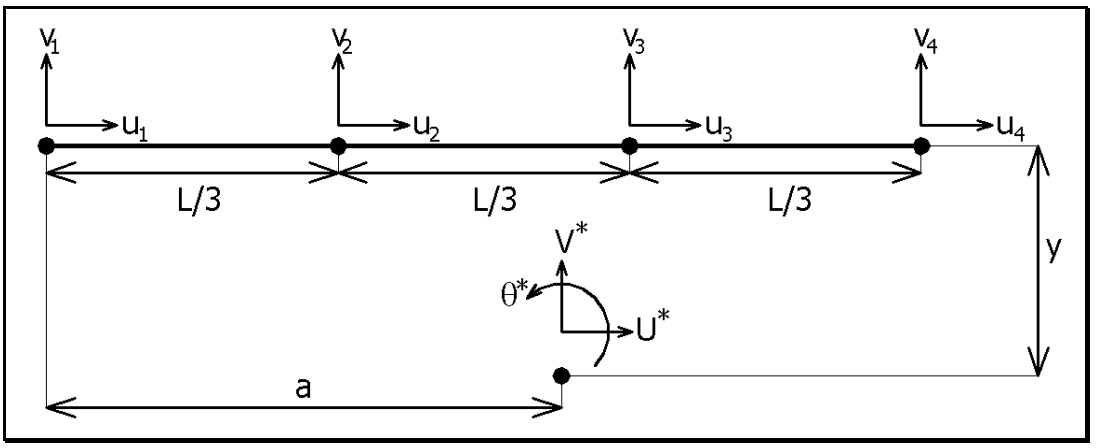

Figure 2.9 Rigid body constraints for interface element

The relation between DOF’s of the node considered and the interface element boundary node DOF’s is given in Equation (2.22).

$$
\begin{aligned}
u_i &= U^* - y\cdot\theta^* \quad (i=1-4)\\
v_1 &= V^* - a\cdot\theta^*\\
v_2 &= V^* - \left(a-\frac{L}{3}\right)\cdot\theta^*\\
v_3 &= V^* - \left(a-\frac{2L}{3}\right)\cdot\theta^*\\
v_4 &= V^* - (a-L)\cdot\theta^*
\end{aligned}
\qquad (2.22)
$$

These constraint conditions can be expressed in the form of a transformation matrix, $\underline{T}(L,a,y)$ as given in Equation (2.23).

$$\underline{T}(L,a,y)=\begin{bmatrix} 1 & 0 & -y \\ 0 & 1 & -a \\ 1 & 0 & -y \\ 0 & 1 & -a+\frac{L}{3} \\ 1 & 0 & -y \\ 0 & 1 & -a+\frac{2L}{3} \\ 1 & 0 & -y \\ 0 & 1 & -a+L \end{bmatrix} \qquad (2.23)$$

2.3.2 Interface Element Tangential Stiffness Matrix

The integral given in Equation (2.26) is evaluated numerically by the Gauss numerical integration to obtain the interface element tangential stiffness matrix $\underline{K}$. In the summation expression, the weight of an integration point $\alpha_{ij} = \alpha_i \alpha_j$ and the position of it, (r_i, s_j), in local coordinate system is obtained by the Gauss-Legendre numerical integration tables. The indices i and j ranges over the number of integration in the r and s directions, respectively. The interface element thickness in the third local direction is taken as w. In this study, the numerical integration in Equation (2.24) is carried out using three points in the r-direction and two points in the s-direction.

$$\underline{K}=\iint_A \underline{B}^T\cdot\underline{D}\cdot\underline{B}\cdot w\ dx\,dy$$

$$\underline{K}=\int_{-1}^{+1}\int_{-1}^{+1} \underline{B}^T\cdot\underline{D}\cdot\underline{B}\cdot w\cdot\left|\underline{J}\right| dr\,ds \qquad (2.24)$$

$$\underline{K}=\sum_{i}^{m}\sum_{j}^{n} {}^{ij}\underline{B}^T\cdot{}^{ij}\underline{D}\cdot{}^{ij}\underline{B}\cdot w\cdot\left|{}^{ij}\underline{J}\right|\cdot\alpha_{ij}$$

2.3.3 Interface Element Response Vector

In the interface element formulation small deformation theory is used and the geometric nonlinearities are not taken into account. Only, material nonlinearities are considered. For a given displacement vector $\underline{U}^*$ the interface displacement vector $\underline{U}$ is computed by using the transformation matrix $\underline{T}$. Then, the response vector $\underline{R}$ is computed by the integral in Equation (2.25). The response vector

calculation is very similar to stiffness matrix calculation. Therefore, a similar procedure is used. The integral is evaluated numerically by Gaussian numerical integration as given in Equations (2.25. The numerical integration is carried out using three points in the r-direction and two points in the s-direction.

$$\underline{R} = \iint_A \underline{B}^T \cdot \underline{\sigma} \cdot w \; dx\, dy$$

$$\underline{R} = \int_{-1}^{+1} \int_{-1}^{+1} \underline{B}^T \cdot \underline{\sigma} \cdot w \cdot \left| \underline{J} \right| dr\, ds \qquad (2.25)$$

$$^{ij}\underline{\sigma} = {}^{ij}\underline{D} \cdot {}^{ij}\underline{B} \cdot \underline{U}$$

$$\underline{R} = \sum_i^m \sum_j^n {}^{ij}\underline{B}^T \cdot {}^{ij}\underline{\sigma} \cdot w \cdot \left| {}^{ij}\underline{J} \right| \cdot \alpha_{ij}$$

2.4 Nonlinear Frame Super Element

A nonlinear frame super element is developed in order to model the behavior of strengthened RC frame members. There are four possible layouts for the frame super elements. The layout possibilities are shown in Figure 2.10 for a frame super element divided into seven segments.

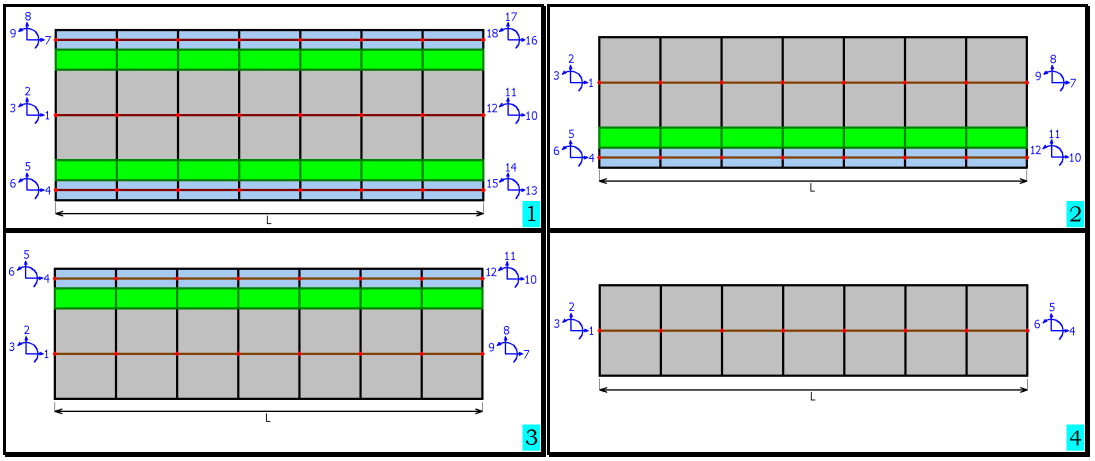

Figure 2.10 Typical frame super elements: (1) with bottom and top strengthening layers; (2) with bottom strengthening layer only; (3) with top strengthening layer only; (4) without any strengthening layers

As seen in Figure 2.10, a frame super element is composed of many frame and interface elements. It should be noted that the interface element DOF's are constrained to corresponding bottom and top frame element DOF's by using the beam constraint equations which are explained in Section (2.3.1.1). There are two

types of nodes in the mesh; internal and boundary nodes. Internal nodes are called the slave nodes and DOF's of slave nodes are condensed. Boundary nodes are called the master nodes and DOF's of master nodes are retained. Consider a frame super element which is divided into N segments. The total number of nodes is (N+1) times the number of layers. The nodal points are numbered from left to right. At each section through the super element, the nodal point of the central frame is numbered first. This is followed by the nodal point of the bottom frame and then the top frame. Based on this node numbering scheme, a DOF mapping vector is generated for each frame and interface element forming the super element. This mapping vector is then used in the assembly stage of the super element stiffness matrix and the response vector. Actually, formation of the stiffness matrix and the response vector is just an assemblage and condensation process. Details of these processes are explained in the following sections.

2.4.1 Frame Super Element Tangential Stiffness Matrix

It was already stated before that a frame super element is composed of many frame and interface elements. The super element manages all the simple elements. It keeps track of the mapping vectors and the current state of each element, etc. This information is utilized in the formation of the tangential stiffness matrix of the frame super element. That is tangential stiffness matrices of all frame and interface elements are formed and assembled into the frame super element stiffness matrix by using mapping vectors. Normally, the size of the frame super element stiffness matrix is three times the total number of nodal points in its FE mesh. However, it is condensed to the boundary DOF's before assembled into the structural stiffness matrix. The final condensed size of the frame super element stiffness matrix is six times the number of layers. The frame super element has a well-defined diagonal matrix topology. The condensation operation is performed by taking advantage of this topology.

2.4.2 Frame Super Element Response Vector

An incremental solution algorithm for the analysis of structural system is utilized in this study. Therefore, the frame super element must keep track of the history of each constituent element. The current formulation necessitates the knowledge of

the cumulative displacement vector of the previous iteration. On a system basis, consider a structure in equilibrium under the applied external loads with the displacement vector ${}^{t}\underline{U}$ at time t. An external disturbance is applied on the system in the time interval [t,t+Δt]. New equilibrium at time t+Δt is established with the displacement vector ${}^{t+\Delta t}\underline{U}$. The new displacement vector ${}^{t+\Delta t}\underline{U}$ is computed by the Newton-Rapson iterations. In these iterations, the i^{th} approximation ${}^{t+\Delta t}\underline{U}^{i}$ is improved by the addition of the incremental displacement $\Delta\underline{U}^{i}$. The structural stiffness matrix may be updated at the beginning of each increment or iteration. The residual load vector $\Delta\underline{R}^{i}$ is the difference between the external disturbance at time t+Δt and the current internal response corresponding to the i^{th} approximation displacement vector ${}^{t+\Delta t}\underline{U}^{i}$. The incremental displacement vector $\Delta\underline{U}^{i}$ is obtained by solving the system of equations $\underline{K}\,\Delta\underline{U}^{i} = \Delta\underline{R}^{i}$.

The frame super element stores the current updated displacement vector of the previous iteration ${}^{t+\Delta t}\underline{U}^{i}$. When the frame super element is subjected to an additional displacement increment $\Delta\underline{U}^{i}$ which is defined in terms of its master DOF's, the corresponding slave node displacement increment is calculated first before the current displacement vector is updated to obtain ${}^{t+\Delta t}\underline{U}^{i+1}$. The recovery of the slave node displacement increments based on the master node displacement increments is defined by Equation (2.27) given in Section (2.4.3). The important point here is that the stiffness matrices $\underline{K}_{ss}$ and $\underline{K}_{sm}$ must be the ones which are used for the computation of the master displacement increments since the static condensation is performed on basis of these stiffness terms. The calculation of the super element response vector is simply a process of calculating the response of each constituent element and assembling them by using the mapping vectors. Similar to the tangential stiffness matrix, the frame super element response vector is also condensed to the boundary DOF's before it is assembled into structural response vector. Note that the condensation of the response vector requires the parts of the frame super element tangential stiffness matrix $\underline{K}_{ms}$ and $\underline{K}_{ss}$, corresponding to slave DOF's.

2.4.3 Condensation of Frame Super Element Internal DOF's

The frame super element tangential stiffness matrix $\underline{K}$ relates the applied load increment $\Delta\underline{F}$ to the resulting displacement increment $\Delta\underline{U}$. DOF's of super element are classified into two groups; the master DOF's denoted by the subscripts m and

the slave DOF's denoted by the subscript s. Then, the equilibrium equations can be expressed as given in Equation (2.26) by partitioning the stiffness matrix $\underline{K}$, the displacement increment vector $\Delta\underline{U}$, and the load increment vector $\Delta\underline{F}$.

$$\underline{K}\cdot\Delta\underline{U}=\Delta\underline{F}$$
$$\begin{bmatrix}\underline{K}_{mm} & \underline{K}_{ms}\\ \underline{K}_{sm} & \underline{K}_{ss}\end{bmatrix}\cdot\begin{bmatrix}\Delta\underline{U}_m\\ \Delta\underline{U}_s\end{bmatrix}=\begin{bmatrix}\Delta\underline{F}_m\\ \Delta\underline{F}_s\end{bmatrix} \qquad (2.26)$$

the condensation of the tangential stiffness matrix $\underline{K}$ and the incremental load vector $\Delta\underline{F}$ given in Equation (2.26) is performed as follows. The slave part of the frame super element displacement vector $\Delta\underline{U}_s$ can be solved in terms of the master displacement vector $\Delta\underline{U}_m$ as given in the Equation (2.27).

$$\Delta\underline{U}_s=\underline{K}_{ss}^{-1}\cdot\left(\Delta\underline{F}_s-\underline{K}_{sm}\cdot\Delta\underline{U}_m\right) \qquad (2.27)$$

Inserting $\Delta\underline{U}_s$ into the first line of Equation (2.26) gives the condensed stiffness relation of frame super element. See Equation (2.28).

$$\underline{K}_{mm}\cdot\Delta\underline{U}_m+\underline{K}_{ms}\cdot\underline{K}_{ss}^{-1}\cdot\left(\Delta\underline{F}_s-\underline{K}_{sm}\cdot\Delta\underline{U}_m\right)=\Delta\underline{F}_m$$
$$\left(\underline{K}_{mm}-\underline{K}_{ms}\cdot\underline{K}_{ss}^{-1}\cdot\underline{K}_{sm}\right)\cdot\Delta\underline{U}_m=\Delta\underline{F}_m-\underline{K}_{ms}\cdot\underline{K}_{ss}^{-1}\cdot\Delta\underline{F}_s \qquad (2.28)$$
$$\underline{K}_{cc}\cdot\Delta\underline{U}_m=\Delta\underline{F}_c$$

2.5 Nonlinear Joint Super Element

Frame structures are built up by connecting beams and columns. The joints must be designed as well as the frame members because the failure of a joint means the failure of all members which are connected to it. Conventional frame analysis programs do not have physical joint elements. These programs implicitly assume all joints as rigid and define them simply as a node for element connectivity. The joints are the most critical parts of the frame structures since they are subjected to the highest shear and moment under the influence of lateral loads. Hence, it is very important to know the stress state in the adhesive layers of strengthened joints. As stated in Section (2.3), separation decided according to the average shear stress in the adhesive layer.

Currently, a new joint strengthening method has been developed and this new method is being tested by in the Department of Civil Engineering at the Middle East Technical University. In this method, rigid triangular steel corner pieces are anchored to the joints of the frame structure in order to increase the size, stiffness and strength of the joint. These steel corner pieces serve the purpose of anchoring the steel/FRP plates at the joint as well as providing a convenient way of connecting the brace elements to the frame structure.

In this study, the joint super elements are categorized into three groups according to their physical behavior. These are labeled as *fully rigid*, *division* and *flexible* joint super elements. Each type is described in detail in the following paragraphs.

Fully rigid joint super elements are used when the corner pieces are both bolted and epoxy bonded to the RC frame. Usage of bolts together with epoxy makes the joint very rigid and strong so that there is no possibility of separation. Hence, the rigid joint assumption in mathematical modeling of this type of joints leads to a negligible error in the results. The rigid joints do not require much computational time since there is no stiffness matrix and response vector calculation. There is only rigid body transformation, which is much faster than stiffness matrix formation and response vector calculation. Typical rigid joint super elements are shown in Figure 2.11.

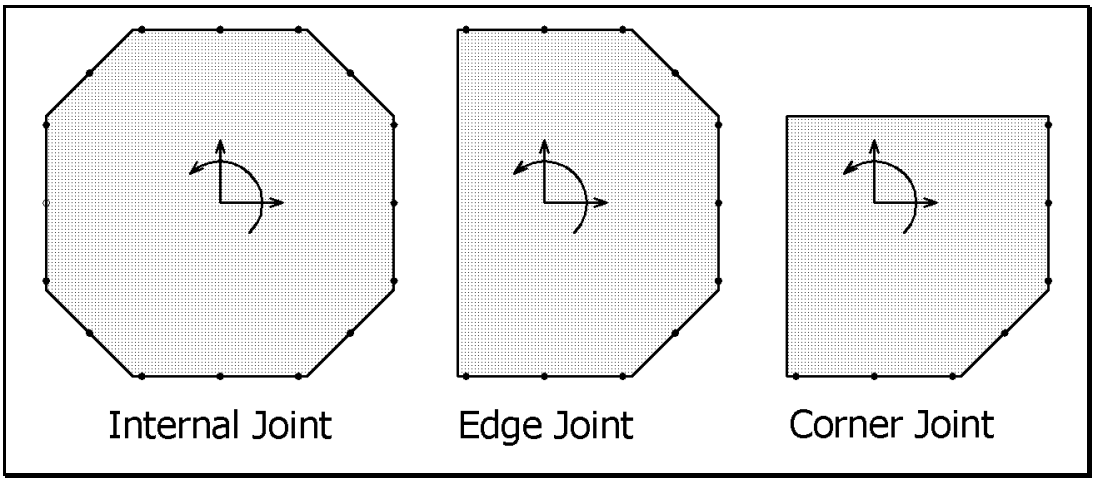

Figure 2.11 Typical rigid joint super elements

The division joint super elements are commonly used to divide a single frame super element into two or more frame super elements. A joint super element is also

considered as a division type if there is only one frame super element connected to it. Actually, division joint super element type is not physical joint. This type of joint super elements is most commonly used to define point loads along the span. In some cases, the user may be interested in the deformations of a point along the span of a frame super element. The division joint super elements are very convenient for these purposes. Typical division joint super elements are shown in Figure 2.12.

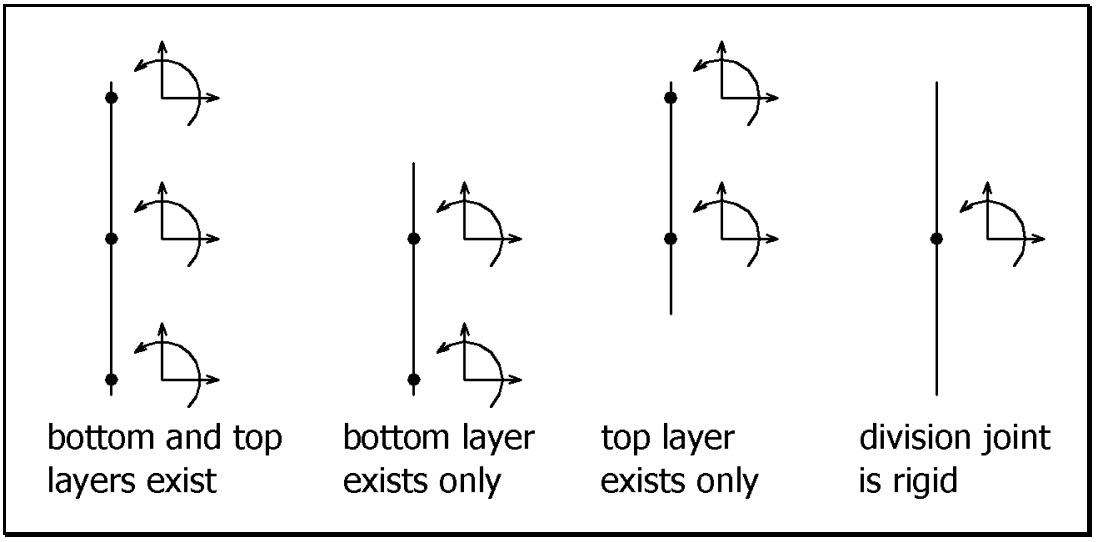

Figure 2.12 Typical division joint super elements

The flexible joint super elements are used when the corner pieces are only epoxy bonded to the RC frame and independent failure of the steel/FRP layers at the joint is anticipated. The use of corner pieces without anchorage bolts carries the risk of having the corner pieces separated from the joint. Therefore, the rigid joint assumption cannot be used in the mathematical modeling of such joints. The flexible joints are computationally the most expensive joint types because they require the formation of a stiffness matrix and the calculation of a response vector. A typical flexible joint super element and its components are shown in Figure 2.13.

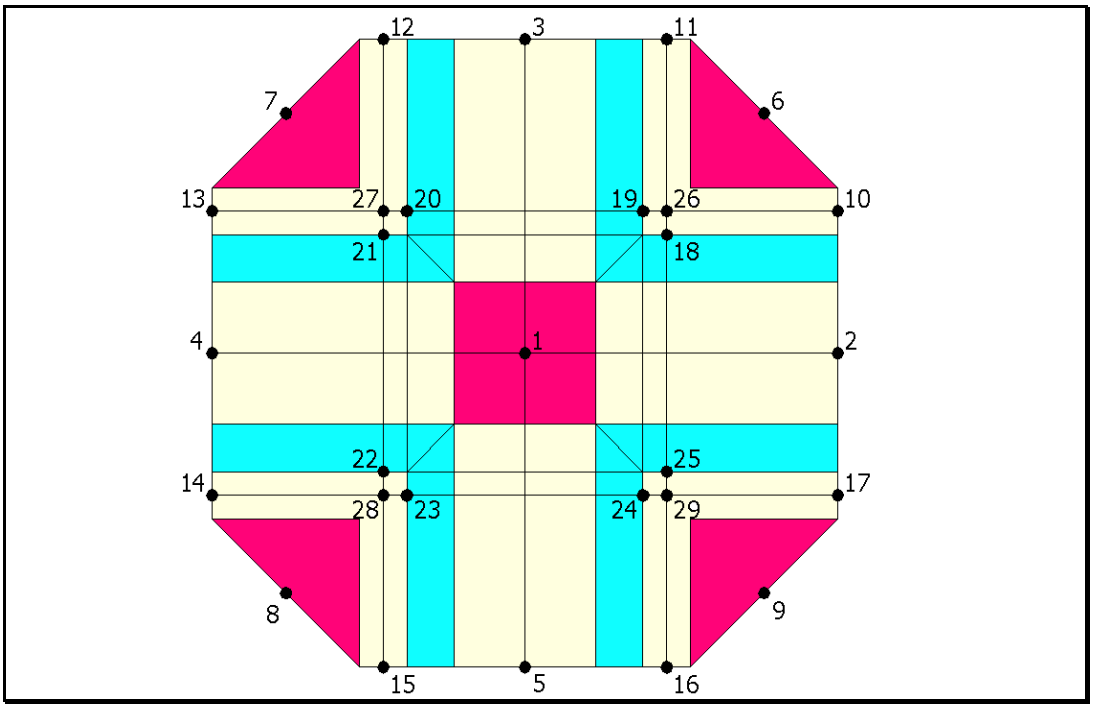

Figure 2.13 A typical flexible joint super element

Joint super elements at different parts of the frame structure, i.e. internal, edge or corner parts, have different layouts. Implementation of the joint super element is performed so as to handle all possible layouts. This flexibility is provided by keeping the record of the internal node configuration of the super element. There are 29 possible locations for the internal nodes which are shown in Figure 2.13. The program determines automatically the existence of internal nodes by using the frame super element connectivity data. DOF numbering of the joint super element is performed accordingly.

Basic constituent elements of the joint super element are the frame elements, the interface elements and the rigid corner pieces. Depending on the anchorage conditions of the rigid corner pieces, the joint super element may be ideally rigid or flexible. The formation of the stiffness matrix, the calculation of the response vector and the process of static condensation is the same as those of the frame super elements. The only difference is the number of master and slave DOF's. Since the DOF numbering is different, there is not a special matrix topology for the joint super elements. However, this does not cause a serious inefficiency as the matrix sizes are very small. The maximum number of total DOF's of a flexible joint super element is 30. The maximum number of master DOF's is 27 and the maximum number of slave DOF's is 9. Furthermore, there is no condensation for

the interior flexible joint super elements since they do not have any slave DOF's. Condensation is required only for edge or corner flexible joint super elements.

2.6 Other Components

Besides the basic finite and super elements described above, the implemented form of the program contains the following classes:

- Material class
- Moment-curvature class
- Section class
- Solver module
- Brace element class
- Structure class

These classes have data structures and special methods in order to manipulate the data structures.

The material class describes an elastic and nonlinear constitutive law. It contains the piecewise linear stress-strain relation and the Poisson's ratio. It has two basic functions. For a given strain state, the first function calculates and returns the stress and the second function calculates and returns the modulus of elasticity.

The moment-curvature class describes the bending behavior of frame elements. It contains the piecewise linear moment-curvature relation data. There are two main methods of the class. For a given curvature state, the first method returns the moment and the second method returns the bending rigidity.

The section class contains the cross-section information of frame super elements. As discussed before, the frame super element contains a RC frame element in the middle and may contain bottom and/or top strengthening plates. The section class contains the cross-section geometry and the mechanical properties.

The solver module contains some global functions for inverting square matrices and for the solution of systems of linear equations. Currently, only LU factorization method is implemented.

Brace element class contains the mechanical and geometric properties of the two frame elements of an x-brace.

Structure object contains all the data and all the methods necessary for the analysis of a structural system. The data arrays of the structure object are for joint super elements, frame super elements, brace elements, moment-curvature relations, sections and materials of the structural system. Additional data for solution method are the number of maximum iterations, the number of loading increments, the convergence tolerance and the convergence criteria to be used. Basic methods of structure object are the input and the output methods, the solver methods, and the assemblage methods.

CHAPTER 3

CASE STUDIES

3.1 A Nonlinear Cantilever Beam without Steel/FRP Plates

A cantilever beam, which has a length of 1000 mm, is analyzed under a tip load of 1.5N. A nonlinear analysis is carried out by using the program and the results are compared with the analytical solution. The geometric properties and the loading of the cantilever beam are shown in Figure 3.1. The cantilever beam has a bilinear moment-curvature relationship as shown in Figure 3.2.

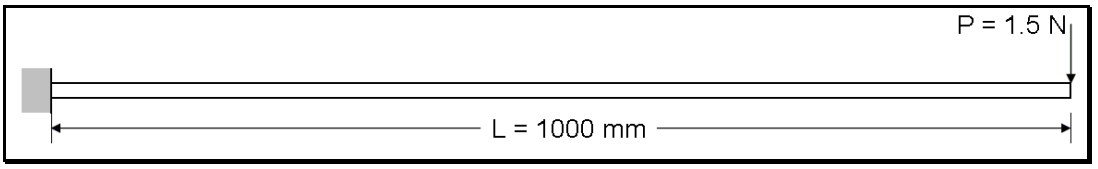

Figure 3.1 Geometric properties of the beam

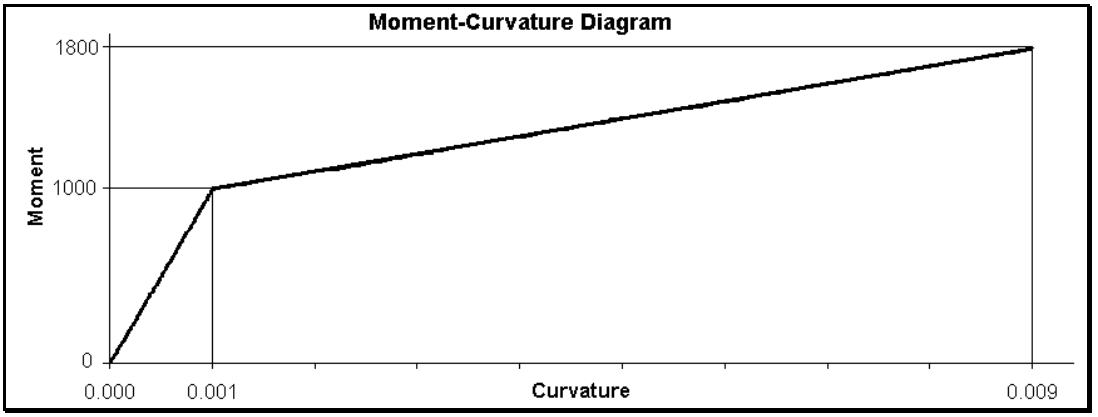

Figure 3.2 Moment-curvature diagram of the beam

The cantilever beam is assumed to be deforming under bending moments only. The shear deformations are neglected. The transverse displacements and the rotation at the tip are found by using the well-known moment-area method. The FE solution obtained by using frame super elements gives the exact solution obtained analytically provided that the curvature diagram is composed of linear segments and the internal (slave) or boundary (master) nodes coincide with the discontinuity (singular) points of the piecewise linear curvature diagram.

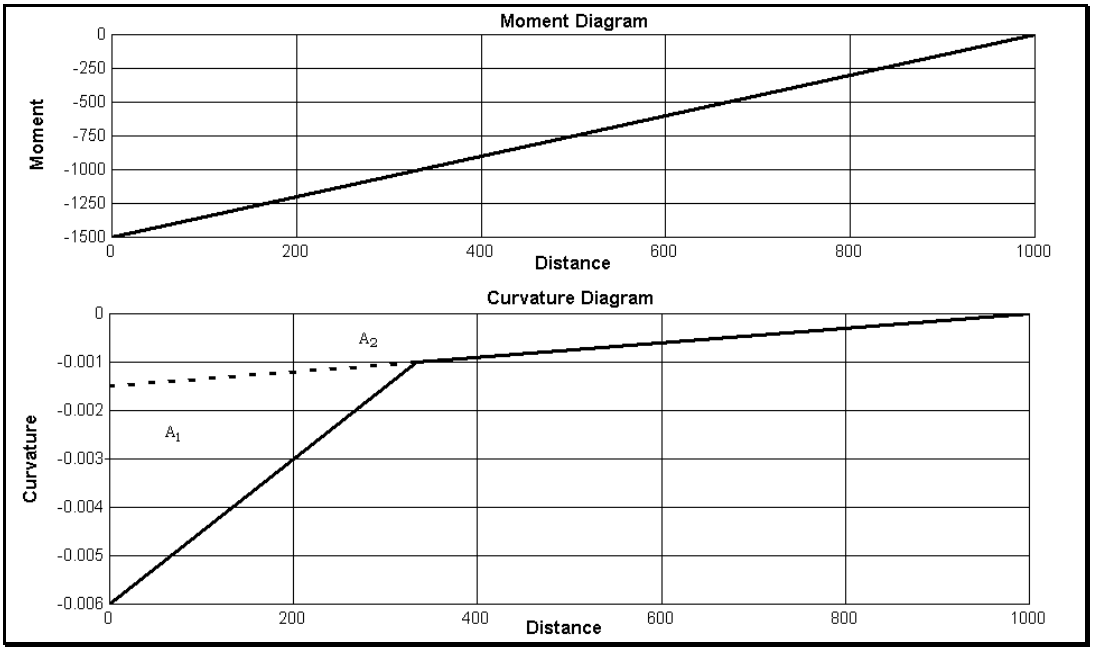

Figure 3.3 Moment and curvature diagrams of the beam for the tip loading

The structure is a statically determinate system and the exact solution can easily be obtained. The moment and curvature diagrams are given in Figure 3.3. Calculation of the tip rotation and the tip deflection of the current cantilever beam by the moment area theorem is given in Equation 3.1 in which r_1 and r_2 are the centroidal distances of the areas A_1 and A_2 from the cantilever tip, respectively

$$\theta = A_1 + A_2$$
$$\theta = \frac{1}{2}\cdot 0.0045 \cdot \frac{1000}{3} + \frac{1}{2}\cdot 0.0015 \cdot 1000$$
$$\theta = 1.5\,\text{rad}$$
$$\Delta = A_1 \cdot r_1 + A_2 \cdot r_2 \qquad (3.1)$$
$$\Delta = \frac{1}{2}\cdot 0.0045 \cdot \frac{1000}{3}\cdot\frac{8000}{9} + \frac{1}{2}\cdot 0.0015 \cdot 1000 \cdot \frac{2000}{3}$$
$$\Delta = 1166.7\,\text{mm}$$

The accuracy of the solution is directly related to how close a master or slave node is to the singular points of the curvature diagram. This can be explained by the fact that the frame super elements are composed of simple frame elements which are exact for linearly varying curvatures. If the curvature does not vary linearly over the frame element, the computed deformations will be approximate. This is verified by this case study. Three different super element meshes as shown in Figure 3.4 are used for this purpose. In Figure 3.4, N represents the number of subdivisions of the corresponding frame super elements.

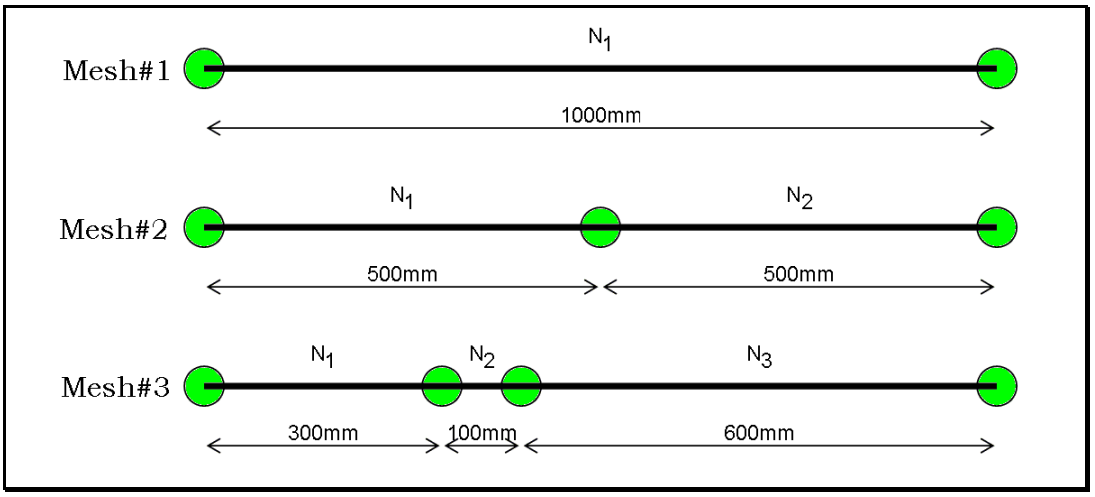

Figure 3.4 Different frame super element meshes for the cantilever beam

The FE code estimations are presented in Tables 3.1-3.3 for the three different super element meshes and the mesh densities.

Table 3.1 Results for the single-super element mesh (Mesh #1).

Mesh 1					
N1	tip deflection (mm)	tip rotation (rad)	Error (mm)	Error (rad)	Closest Distance (mm)
1	1149.5	1.5736	17.2	0.0736	333.3
3	1166.7	1.5000	0.0	0.0000	0.0
4	1136.4	1.4582	30.3	0.0418	83.3
5	1148.0	1.4700	18.7	0.0300	66.7
6	1166.7	1.5000	0.0	0.0000	0.0
7	1156.9	1.4860	9.8	0.0140	47.6
10	1161.8	1.4930	4.9	0.0070	33.3
32	1171.5	1.5073	4.8	0.0073	10.4

Table 3.2 Results for the two-super element mesh (Mesh #2).

Mesh 2						
N1	N2	tip deflection (mm)	tip rotation (rad)	Error (mm)	Error (rad)	Closest Distance (mm)
1	1	1187.2	1.5184	20.5	0.0184	166.7
3	1	1166.7	1.5000	0.0	0.0000	0.0
1	3	1187.2	1.5184	20.5	0.0184	166.7
10	1	1165.4	1.4981	1.3	0.0019	16.7
1	10	1187.2	1.5184	20.5	0.0184	166.7

Table 3.3 Results for the three-super element mesh (Mesh #3).

Mesh 3							
N1	N2	N3	tip deflection (mm)	tip rotation (rad)	Error (mm)	Error (rad)	Closest Distance (mm)
1	1	1	1167.1	1.5007	0.4	0.0007	33.3
3	1	1	1167.1	1.5007	0.4	0.0007	33.3
1	3	1	1166.7	1.5000	0.0	0.0000	0.0
1	1	3	1167.1	1.5007	0.4	0.0007	33.3
10	1	1	1167.1	1.5007	0.4	0.0007	33.3
1	10	1	1166.6	1.4999	0.1	0.0001	3.3
1	1	10	1167.1	1.5007	0.4	0.0007	33.3

It is seen that the magnitude of the error depends on the closest nodal distance from the singular points piecewise linear curvature diagram as shown in Figure 3.5 and 3.6. The solutions with Mesh #2 and Mesh #3 prove that if the increase in the mesh density does not change the closest nodal distance to the singular points, there will be no improvement in the results.

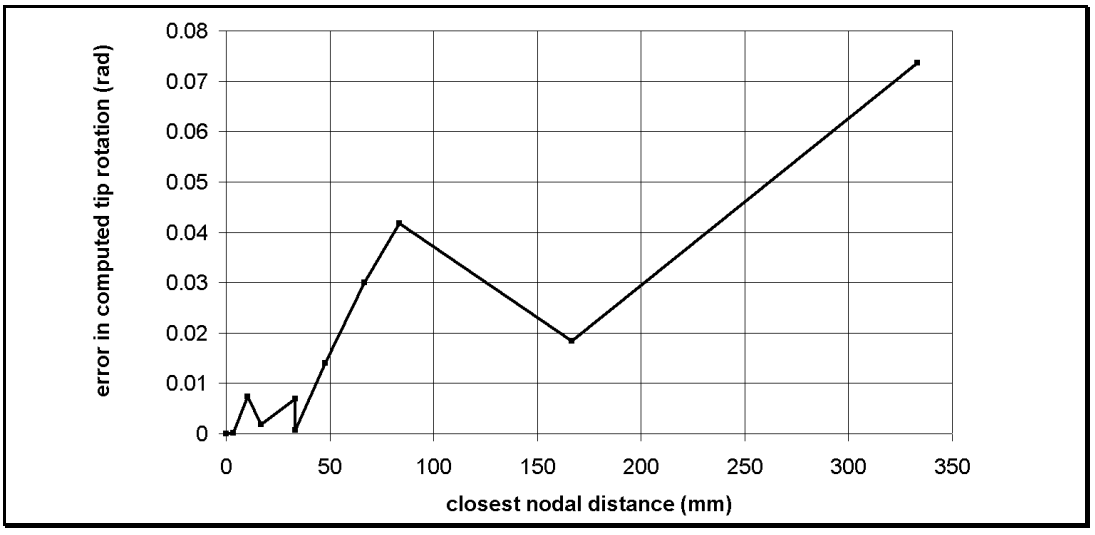

Figure 3.5 Variation of error in rotation against closest nodal distance

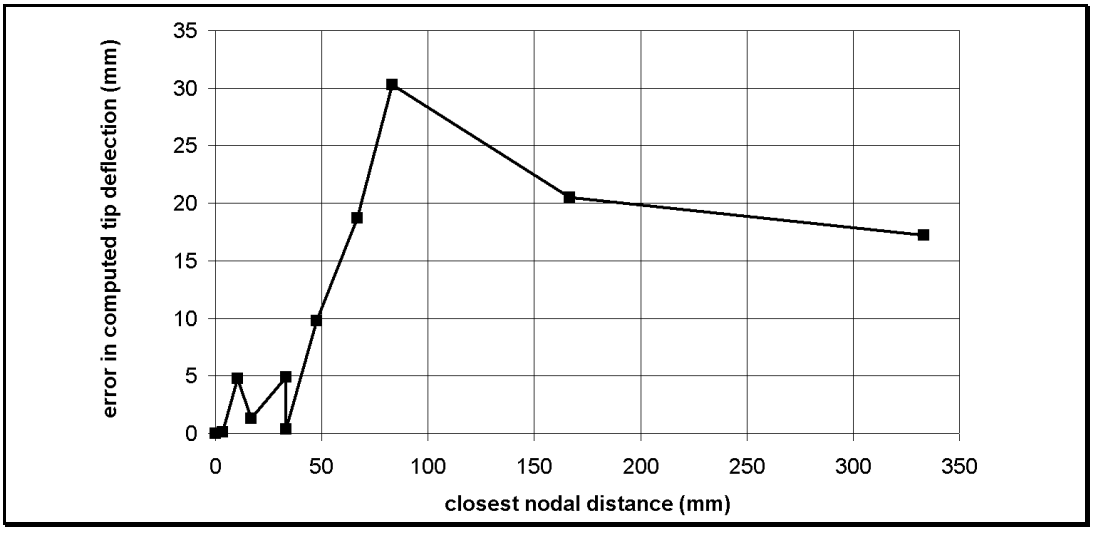

Figure 3.6 Variation of error in deflection against closest nodal distance

The fluctuations in Figures 3.5 and 3.6 are mainly due to the integration point layouts. In some cases, although the closest nodal distance is large, the layout of the integration points is such that the curvature distribution over the beam is better approximated. The fluctuation patterns may be different for deflection and rotation. This can be explained with the help of moment area theorem. Recall that the rotation is related to the area under the curvature diagram and the deflection involves the first moment of the same area. Some curvature approximation may be good for the rotation calculation while it may not be so good for the deflection calculation.

3.2 A Linear 1-Bay, 2-Storey Frame Strengthened with Steel/FRP Plates

A 1-bay, 2-storey frame structure strengthened with steel/FRP plates is analyzed next in order to verify the use of the program for such structures. A linear analysis is carried out and the results are compared with those of SAP2000 [27]. The geometric properties and the loading of the physical frame structure are shown in Figure 3.7. In the figure, all dimensions are given in centimeters. The steel plates which are used at the joint regions are 1 cm thick and epoxy bonded to the RC beam and column faces. The triangular steel corner pieces are 25×25 cm in size and they are both bolted and epoxy bonded to the RC frame elements.

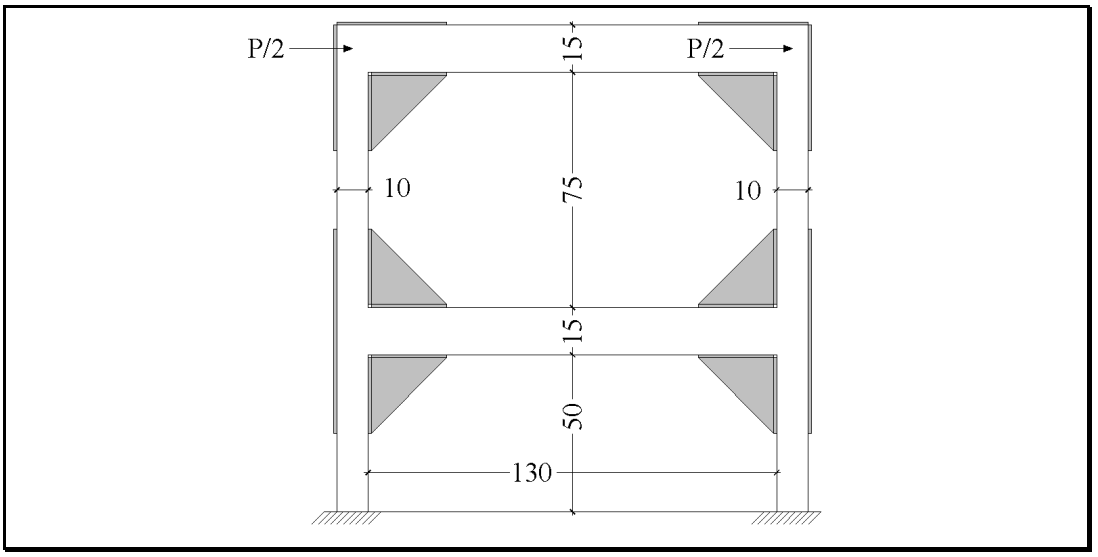

Figure 3.7 Geometric properties of the frame structure

The frame structure is analyzed under the influence of a lateral load at top storey level. Both of the models, the SAP2000 model and the super element model, of the structural system are to represent the same physical problem. The only difference between the two models is in the representation of the interface layer.

The analysis of the frame structure is performed under the following assumptions.

- Shear deformations of the frame members are ignored.
- Joints, including corner pieces, stay rigid during deformations.
- Frame supports at floor level are considered as fix supports.
- A linear analysis is carried out by using initial bending and axial rigidities.

The SAP2000 model is constructed by using frame and shell elements. There are mainly four different materials in the model. First material type is for the RC beams and columns. The second type is for the epoxy layer. The third type is for the steel/FRP plates and the final type is a fictitious material which is nearly rigid. There are mainly four frame and one shell sections in the model. Two of the frame sections are used for the beams and the columns. One is used for the steel/FRP plate and he final fictitious one is used for the simulation of the constraint conditions. Four different FE meshes are used in SAP2000 models. These are shown in Figure 3.8 and the details are given in Table 3.4.

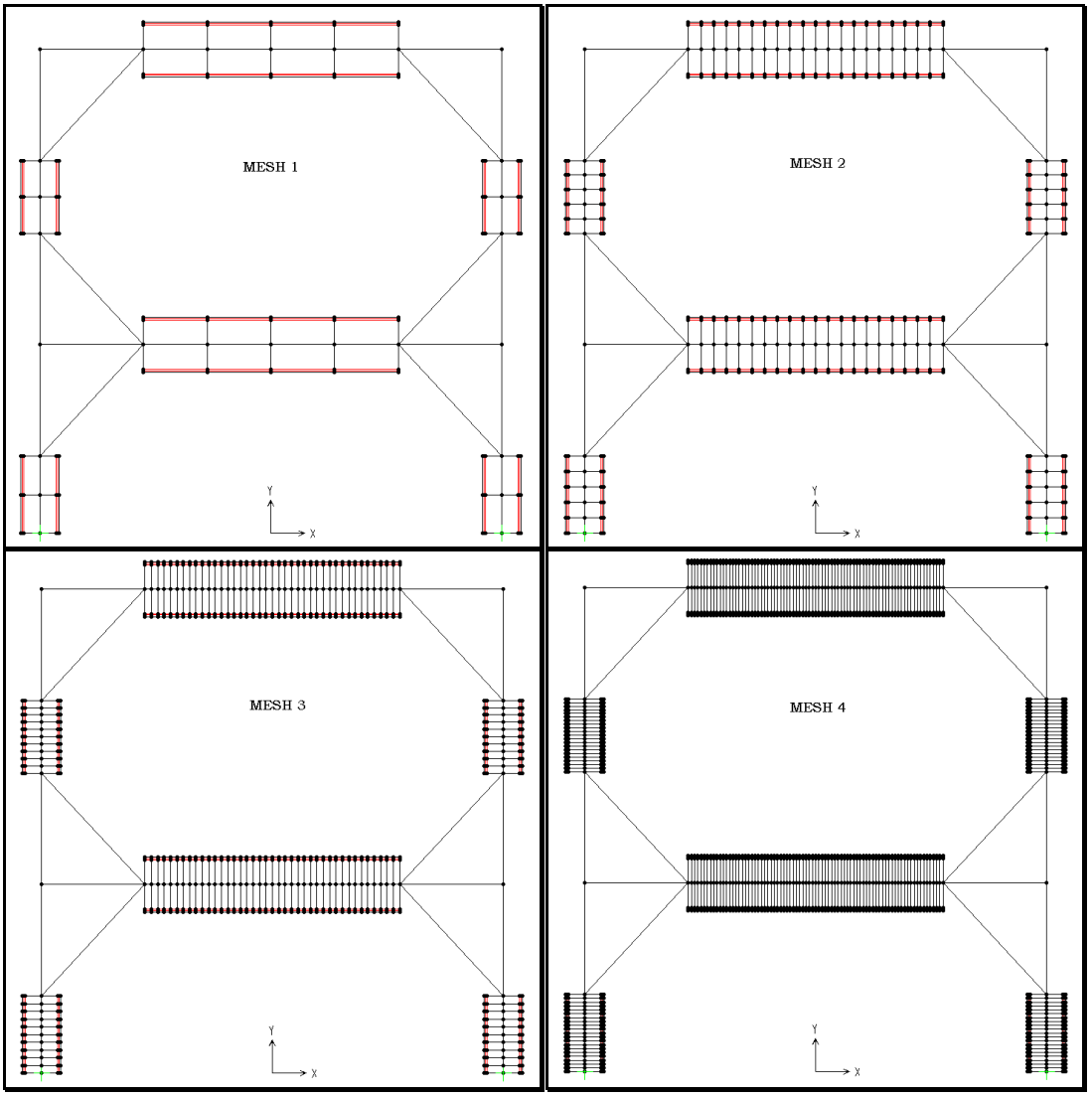

Figure 3.8 Different FE meshes of the strengthened frame for SAP2000 model.

FE model with super elements of this study is constructed by using the same material and section properties as the SAP2000 model to simulate the same conditions. Again, four different mesh densities are considered as shown in Figure 3.9 and the details are given in Table 3.4.

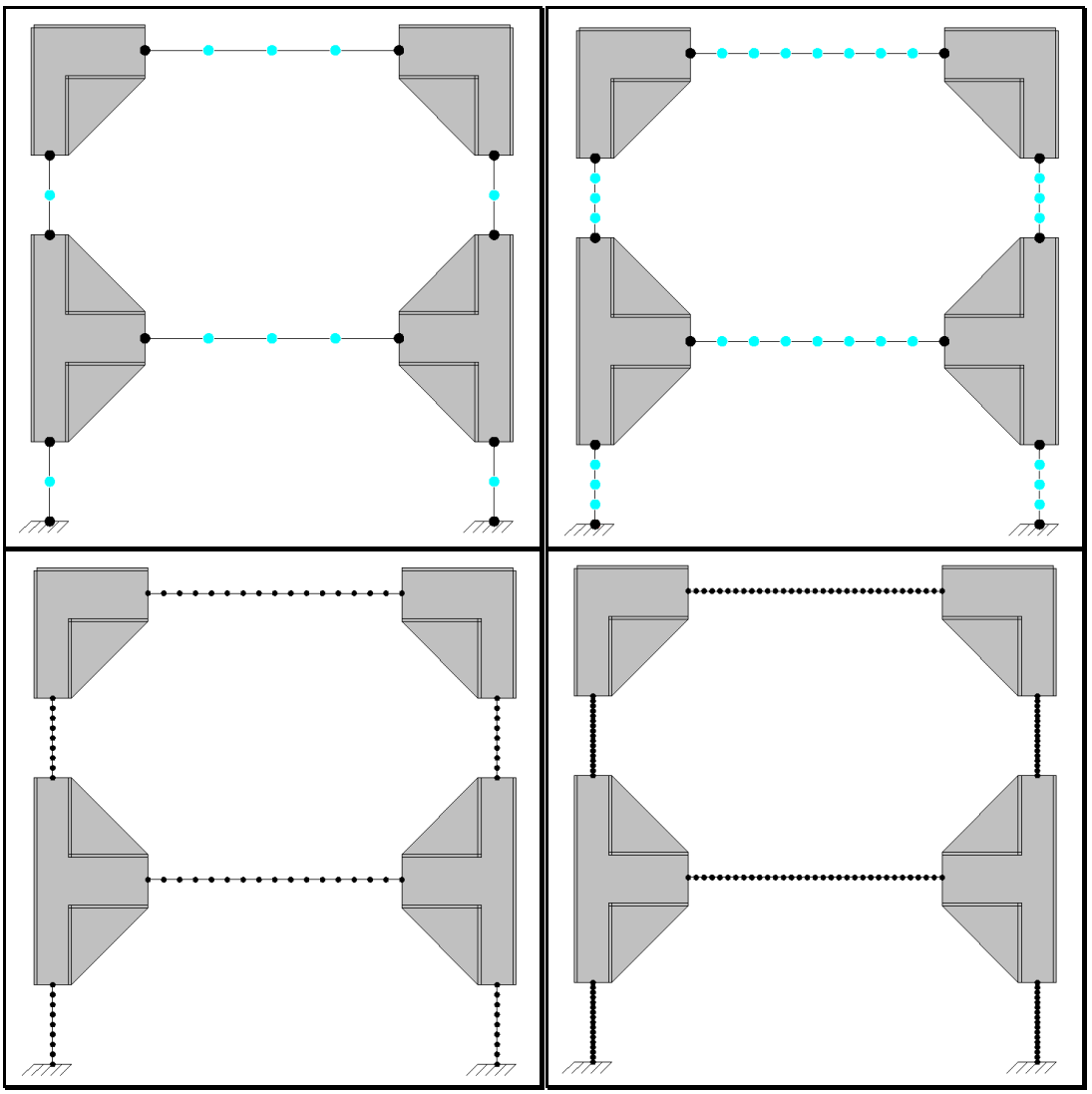

Figure 3.9 Different FE meshes of the frame structure for super element model

Table 3.4 FE mesh details of the models

	Number of divisions			
	SAP2000 Model		Super Element Model	
	Beams	Columns	Beams	Columns
MESH 1	4	2	4	2
MESH 2	20	5	8	4
MESH 3	40	10	16	8
MESH 4	80	20	32	16

The results obtained from both the SAP2000 and the super element models are presented in Table 3.5. Examination of the table reveals that the trend of the SAP2000 model predictions as a function of mesh density is somewhat

unexpected. The system appears to be stiffening as the mesh density increases. This behavior is due to the shell element formulation of SAP2000. It uses a hybrid shell element formulation and, unlike the conventional displacement based FE's, the stiffness of the system increases with the increasing mesh density.

Table 3.5 Displacement predictions of SAP2000 and super element models

		Displacements of 1st Storey			Displacements of 2nd Storey		
		Lateral Displacement (mm)	Vertical Displacement (mm)	Rotation (rad)	Lateral Displacement (mm)	Vertical Displacement (mm)	Rotation (rad)
SAP2000	MESH 1	0.9714	0.08983	0.00169	2.3916	0.12109	0.001090
	MESH 2	0.8423	0.09023	0.00155	2.1006	0.12136	0.000997
	MESH 3	0.8261	0.09025	0.00154	2.0680	0.12137	0.000992
	MESH 4	0.8215	0.09026	0.00154	2.0587	0.12137	0.000991
Super Element	MESH 1	0.735	0.0882	0.00142	1.86	0.118	0.000912
	MESH 2	0.782	0.0881	0.00148	1.96	0.118	0.000951
	MESH 3	0.793	0.0882	0.00149	1.99	0.119	0.000960
	MESH 4	0.795	0.0882	0.00150	1.99	0.119	0.000962

3.3 Nonlinear Simply Supported Beams Strengthened with Steel/FRP Plates

In this case study, the program predictions for a simply supported beam strengthened with externally bonded steel/FRP plates are compared with the experimental and analytical data available in the literature [23, 24].

In the experimental program, a total of seven specimens were tested. All specimens were 3,200-mm long. The longitudinal reinforcement steel ratio was 0.56% and 6-mm-diameter steel stirrups were used as transverse reinforcement with 100-mm spacing. Three beams were strengthened with steel plates and three beams were strengthened with FRP plates. The last beam without any strengthening was used as the control specimen. The reinforcement plates were 50 mm wide. The steel and FRP plates were 4.0 and 1.2 mm thick, respectively. For the plate bonding, the concrete surface was polished and an approximately 2-mm-thick layer of epoxy resin was applied. The specimen geometry and the test layout are shown in Figure 3.10 and the mechanical properties of the materials are summarized in Table 3.6.

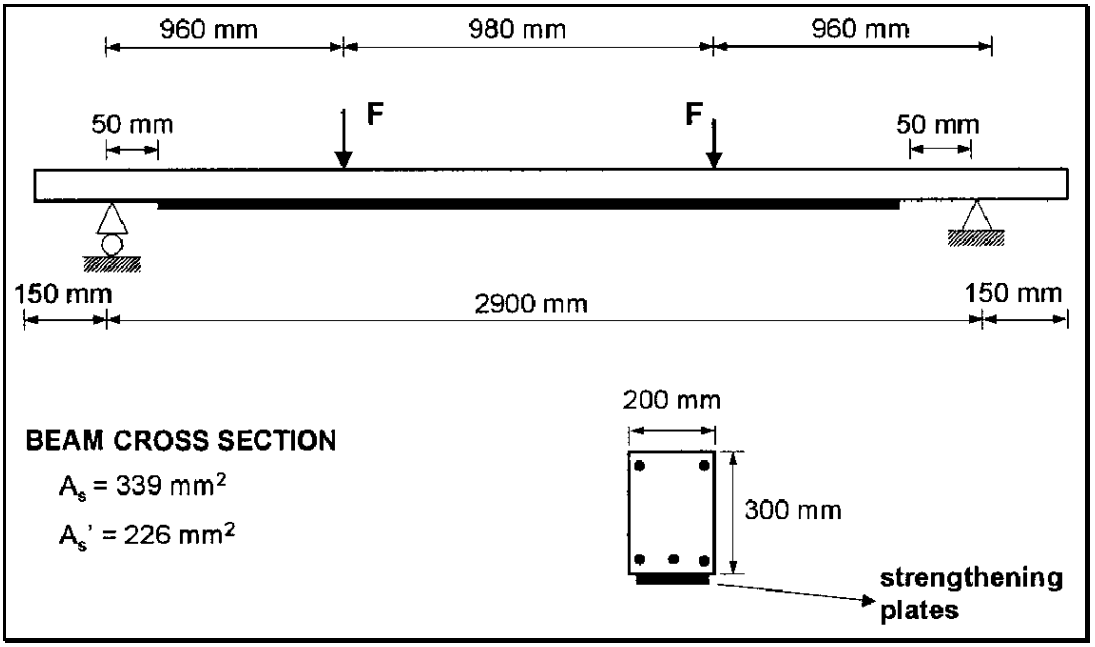

Figure 3.10 The specimen geometric properties and the test layout

Table 3.6 Mechanical properties of the materials, A. Aprile, et al. [24]

Parameter	Elastic modulus (GPa)	Poisson's ratio v	Compressive strength (MPa)	Tensile strength (MPa)
Concrete	27	0.2	25	3.5
Steel bars	210	0.3	460	460
Steel plate	210	0.3	360	360
CFRP plate	150	0.33	—	2,400
Epoxy resin	12.8	0.35	100	4[a]

[a]Adhesion for concrete surface.

A FE mesh containing a total of 3 frame super elements and 4 joint super elements as shown in Figure 3.11 is used to obtain the load–midspan deflection response. The support on the left end restrains the vertical displacement and the support on the right end restrains the horizontal displacement and the rotation. The frame super elements 1, 2 and 3 are divided into 2, 32 and 16 subdivisions, respectively.

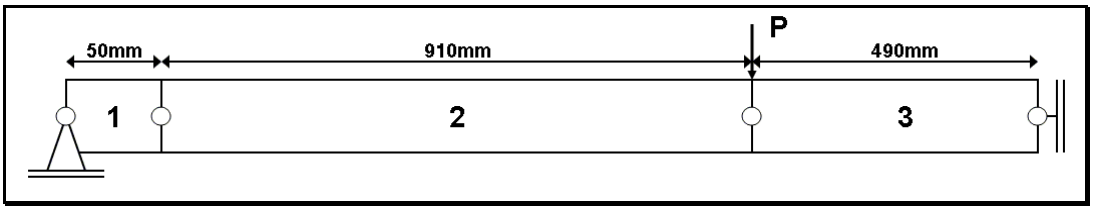

Figure 3.11 The FE mesh of the beam for super element solution

The developed FE code performs the nonlinear analyses by using a force-controlled loading and a Newton-Raphson solution procedure. The interface material model is considered as linear elastic up to failure. This assumption is based on the actual elastic properties of the epoxy resin used for the connection, whereas the failure condition is mainly dependent on the concrete strength and surface preparation. Chajes et al. [25] presented a detailed study on the bond strength of concrete-FRP glued joints subjected to shear stresses.

The results are presented graphically in figures 3.12-3.17. In Figure 3.12, the experimental and numerical results [23] for the specimens are shown on the left and the results obtained by the current program are shown on the right. A few meaningful points are labeled on the curves. Point C marks the onset of concrete cracking in the middle third of the beam and is followed by a drop in the beam stiffness. Point E represents a generic point during loading at which cracking spreads toward the beam support but the bottom steel rebars are still elastic. At point Y_b the bottom steel rebars yield, leading to a further drop in the response stiffness. For the case of the RC beams strengthened with the steel plate, Y_p indicates the point where the steel plate yields. As expected, the plate yields (point Y_p) before the longitudinal reinforcement yields (point Y_b). After the longitudinal reinforcement yields in the steel-strengthened and in the control beams, the response stiffness is very small and mainly due to the hardening properties of the reinforcement steel. On the contrary, for the beams strengthened with FRP plates, after point Y_b the response stiffness is still considerable because of the elastic contribution of the strengthening plate. At point D plate debonding occurs. One can observe from the figures that after point D both the experimental and the numerical responses show a large drop in beam strength because of the loss of the plate contributions. The residual strength is that of the original, non-strengthened RC beams.

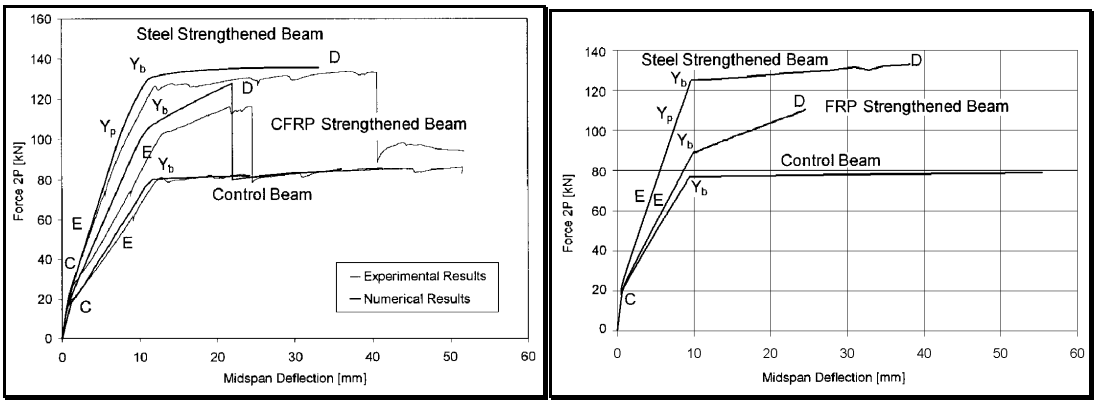

Figure 3.12 Load-midspan deflection curves

The plate tensile force variations in the FRP- and steel-strengthened beams are shown in Figures 3.13 and 3.14, respectively. The different curves refer to the load levels labeled E, Y_p, Y_b, and D. As expected, the force in the plate is zero at the plate end (at 200 mm from the beam end), it increases up to the maximum value reached at the load application point (at 1,100 mm from the beam end), and it remains constant in the middle third of the beam, where the bending moment is constant. Two points on the force distribution curve mark a clear change in the slope between the plate end and the point of load application. The first point, labeled c in Figure 3.13, separates the cracked (to the right of c) from the uncracked sections (to the left of c) of the RC beam. Note that the cracking never reaches the plate end section because the failure by plate debonding occurs first. The second point, labeled y_b in Figure 3.13, corresponds to the section where the bottom steel rebars yield. The rebars are yielded to the right of point y_b and are still elastic to the left of it. Point y_b moves to the left as the load level is increased from level Y_b to level D, indicating the yield penetration as the load increases.

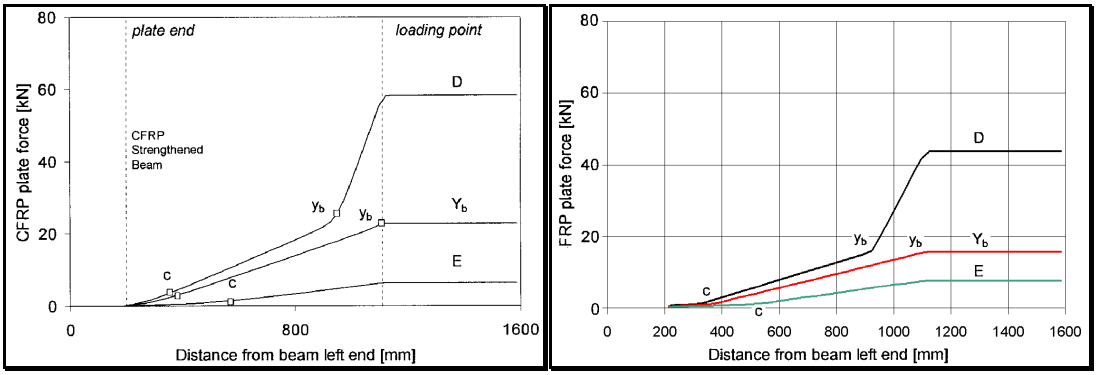

Figure 3.13 Variation of tensile force in FRP plate

If we now consider the case of the force distribution in the steel strengthening plate (Figure 3.14), note that the force in the steel plate cannot increase after yielding and the force maximum value is reached at load level Y_p whereas the force in the CFRP plate keeps on increasing until debonding occurs at load level D. Point y_p in Figure 3.14 separates the region where the steel plate has already yielded (to the right of y_p) from the region where the plate steel is yet to yield (to the left of y_p).

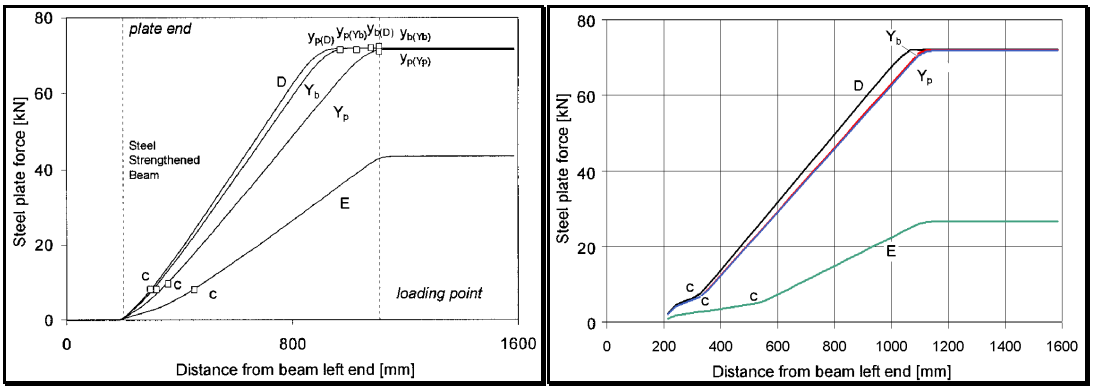

Figure 3.14 Variation of tensile force in steel plate

The bond force distributions in the beam with CFRP plate and beam with steel plate are shown in Figures 3.15 and 3.16, respectively. It is worth recalling that the bond force is proportional to the derivative of the force in the plate. Consequently, the bond stress is zero in the center third of the beam, where the shear force is zero.

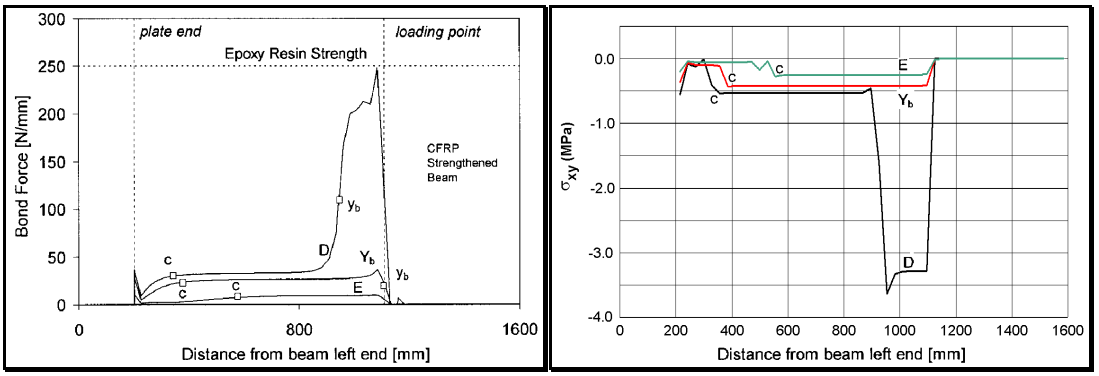

Figure 3.15 Bond force and stress distribution for FRP-strengthened beam

From the comparison of Figure 3.15 and 3.16, it is observed that the bond force distribution for the steel and the FRP plates are quite different. For the FRP strengthened beam, starting from the point where the load is applied and moving to the left towards the beam support, the bond force distribution gradually

decreases except for two main points of discontinuity: one at the plate end and the other near the loading point. The bond discontinuity at the free end, due to the sudden change in the cross section, is a well-known phenomenon; among the many studies available in the literature. The bond discontinuity at the load application point is due to the sudden drop in the plate tensile force outside the region of constant moment. This bond discontinuity becomes sharper as larger loads are applied, but the largest increases are due to the rebar yield penetration along the beam. More specifically, for the bond force distribution corresponding to load level E, bond increases sharply near the point of load application and then decreases up to point c, which separates cracked and uncracked regions. The bond force drops to almost zero at point c. At loading level Y_b, the bond distribution drops drastically after the peak point (near the load application point) and remains constant over the cracked region where the steel rebars are still elastic. A similar bond force distribution is observed at load level D, but the bond force values are larger and there is a short plateau of almost constant bond after the peak. This plateau, which corresponds to the region where the bottom steel has yielded, ends roughly at point y_b, beyond which the bottom steel is still elastic.

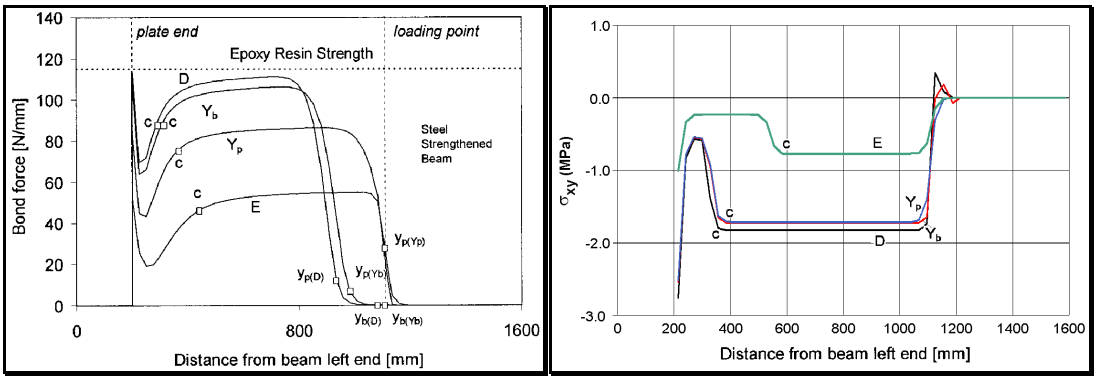

Figure 3.16 Bond force and stress distribution for steel-strengthened beam

The bond force distributions for the steel-strengthened beam are shown in Figure 3.16. In this case, the bond force is zero near the load application point, up to the point y_p, which marks the separation between yielded and non-yielded steel plate. Directly to the left of point y_p, the bond force sharply increases from zero to an almost constant value until point c, beyond which the concrete is uncracked. Finally, a sharp discontinuity arises at the plate end, which in this case represents the maximum bond value for the total length of the plate. As the load level increases, the plate steel yield front (point y_p) moves to the left and, consequently, the bond discontinuity and the intermediate plateau values increase too. This bond

force increase is due to the shortening of the plate anchorage length, which spans from point y_p to the plate end. As steel yielding penetrates towards the plate end, the anchorage length decreases and the bond forces must increase to maintain equilibrium.

Variation of normal stress σ_{yy} along the interface of steel/FRP plates and RC beams at different load levels is given in Figure 3.17. The figure on the left side is for FRP strengthened beam and the one on the right is for steel strengthened beam.

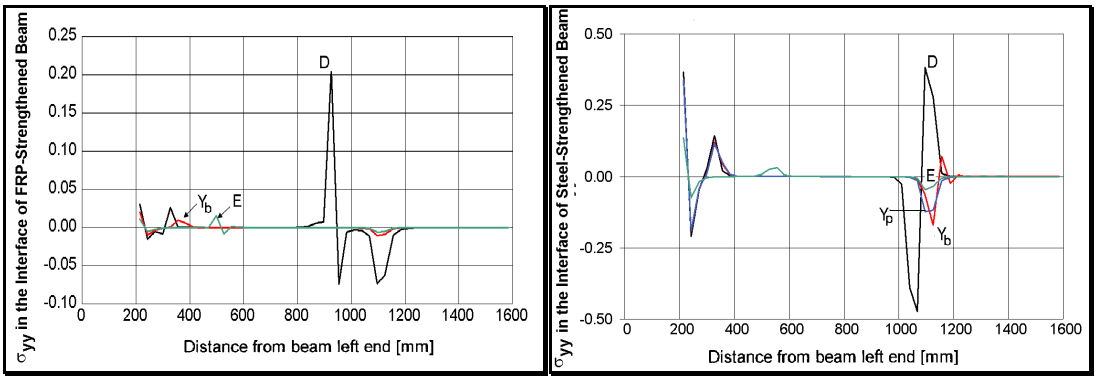

Figure 3.17 Variation of normal stresses in the interface

CHAPTER 4

SUMMARY, DISCUSSION OF RESULTS AND CONCLUSIONS

4.1 Summary

In this study, a special purpose layered frame super element, a joint super element, a frame element and an interface element are formulated and implemented into a nonlinear finite element program for the analysis of frame structures strengthened with externally bonded steel/FRP plates. Frame and joint super elements make the analysis of strengthened frame structures easier and more accurate compared to commercially available general purpose FE packages, which use standard and simple elements.

The main purpose of the current study is to generate a tool for the engineers for predicting the failure load, the failure modes, the region of separation, etc. in such structures. Previous analytical and experimental works performed on steel/FRP strengthened RC frame structures are selected with care. Many of the analytical studies try either to formulate new interface elements to predict the separation of steel/FRP plates or to develop an analytic expression for the stress and strain variation in the adhesive layer. Many of the experimental studies are performed either to measure the load deflection characteristics of the strengthened beams or to determine the steel/FRP to the RC bond characteristics. A detailed description and the main components of each study are given in this chapter.

In chapter 2, the formulation of the basic elements and super elements for the current study is given. The basic elements are the frame and interface elements. The super elements are the frame and the joint super elements. The frame element

uses the moment-curvature relation as constitutive law for the bending behavior and stress-strain relation for the axial behavior. The frame element uses a transformation matrix for the imposition of rigid end zones. The interface element has a material model which is linear elastic up to failure. The interface elements are placed either in between two frame elements or a corner piece and a frame element for the modeling of adhesive layer. The displacement fields of these elements must be compatible with the connected elements. This compatibility is provided by the beam and rigid body constraint equations. The failure of the interface element is decided according to the average shear stress in the element. The frame super element knows the connectivity of its basic elements so that it can form its stiffness matrix and calculate its response vector. The frame super element uses the static condensation in order to eliminate its internal DOF's. The joint super element has the same structure with that of the frame super element except for the joint super element has a more complex FE discritization which requires extra care in the implementation. Brace elements are not super elements. They contain two crossing simple frame elements for the simulation of x-braces.

In chapter 3, there are three case studies. Each case study is designed and carried out in order to test the performance and correctness of the super elements. The first case study is a nonlinear cantilever beam problem for which analytical solution is known. The second case study is a linear 1-bay, 2-storey strengthened frame structure. The frame structure is analyzed by using both the developed program and SAP2000. The third case study is a nonlinear simply supported strengthened beam. The force-displacement, the plate tensile force distribution and the adhesive stress distribution curves which are represented by Aprile et al [23, 24] for the strengthened RC beams by externally bonded steel/FRP plates are compared with those obtained by the developed program. All the explanations and comparisons of the results are performed in tabular or graphical forms.

4.2 Discussion of Results and Conclusions

The first case study is designed to verify the accuracy of the frame super element without any steel/FRP plates. For this purpose, a hypothetical cantilever beam loaded at the tip is considered with a bilinear moment curvature relation. The comparison of the program estimation and the analytical solution reveals that the frame super element has the capability of predicting the stress and displacement

fields correctly. Note that the exact response is predicted as long as the internal or boundary nodes of the frame super elements coincide with the rigidity changing points of the curvature diagram. The errors in the approximations for tip deflection and rotation by using three different super element meshes with different subdivisions are plotted against the closest nodal distance to such points. The fluctuations in the predicted response values are mainly due to the integration point locations over the cantilever beam structure. In some meshes, the layout of the integration points is such that the curvature distribution is better approximated. As a result, the fluctuation patterns for deflection and rotation response may be different since some curvature approximations may be good for the rotation calculation while it may not be so good for the deflection calculation. It is verified by this case study that the FE code developed in this study can be used for the nonlinear analysis of RC beams or frame structures.

In the second case study, the FE code is used for the analysis of a frame structure which is strengthened by externally bonded steel/FRP plates. The super element and SAP2000 approximations are compared with each other. It is observed that the stress and displacement field approximations are very similar. Solutions obtained from both programs are convergent as the mesh density increases. However, the super element convergence rate is much faster with increasing mesh density. Examination of the SAP2000 results reveals that the trend of the system appears to be stiffening as the mesh density increases. This behavior of SAP2000 is due to its shell element formulation. On the other hand, the interface element of the current study uses conventional displacement based FE formulation. Since the displacement based FE's are weak for stress field estimations, the average shear stress is in each interface element is used in the failure criteria for adhesive layer instead of the integration point values which vary drastically from one point to another in the same element. The nodal displacements related to axial deformation of the frame elements can be obtained accurately with a minimum number of super element subdivisions. However, a fine mesh must be used for an accurate prediction of the flexural response. The preparation of the computer models of such structures is a time consuming and error prone process. The current program utilizes an easy to prepare text input file and easy to understand text output file. However, one has to manipulate the output text file to obtain visual graphs for stress and force variations over the super elements of the structure.

The final case study involves the nonlinear analysis of a simply supported beam strengthened by externally bonded steel/FRP plates. The program estimations are compared with experimental data available in the literature [23, 24]. The developed FE code yields a good estimation of both the stiffness and the strength of such strengthened beams. A close agreement is observed between the experimental data and the program predictions for the load-midspan deflection curve. In addition, the variation of the stress states in the interface layer and the variation of the axial load in the strengthening plate at different load levels are in good agreement with the experimental and analytical data in the literature. The displacement field of the interface layer is accurately and smoothly estimated by the polynomial shape functions of the interface element. However, this accuracy is lost in the computation of the strain field which is obtained through the use of shape function derivatives. Accordingly, the computed stress field in the interface element is not smooth. This inconvenience is overcome by using an average stress definition within the interface element. It is verified by this case study that the developed program can be used as an efficient tool for the nonlinear analysis of frame structures strengthened with externally bonded steel/FRP plates.

In the light of all the results obtained from the case studies and the observations made in the course of this study, the following general conclusions about the frame and joint super elements, the frame and interface elements, and the FE code can be stated.

- The nonlinear frame super element of this study can predict accurately the stress and displacement response of the actual frame members with or without externally bonded steel/FRP plates.
- The failure modes such as plate separation, yield and rupture and the failure regions in a RC frame structure strengthened by externally bonded steel/FRP plates can be predicted by the use of the super elements formulated in this study
- The locations of plastic hinges forming in the beams or columns of a bare RC frame structure can be identified and the load levels at which these hinges form can be determined by the nonlinear frame super elements.
- The nonlinear frame super element can also be used for the nonlinear analysis of steel frame structures if the moment-curvature relation for the steel section is supplied instead of that of the RC section.

- The frame and the joint super elements formulated and implemented in this study are very practical tools for the analysis of large structural systems.
- The FE code assembled in this study based on the nonlinear frame and joint super element and the interface element is a valuable tool for the effective and efficient nonlinear analysis of RC or steel frame structures.

4.3 Recommendations for Future Studies

Never-ending advances are being realized in the composite materials technology, computer science and FE technology. In order to develop a high performance FE program, one must make use of the high technology and utilize not only science and imagination but also inspiration. Programming is a never-ending task. Therefore, the following future studies are suggested for the enhancement and improvement of the developed FE analysis program.

- The frame element stiffness matrix and response vector can be evaluated numerically with varying number of Gauss integration points. This will enhance the element for non-prismatic sections, and distributed plasticity over the frame element.
- A new strip element, which will be cheaper than the nonlinear frame element, may be developed for the FRP plates since their bending rigidities are negligibly small as compared to those of RC beams.
- Besides the already implemented x-bracing, other types of bracings may be implemented to form a bracing library in the program.
- A parametric study may be performed to represent the infill walls with an equivalent brace element.
- Frame super element stiffness matrix has a special topology. It will be very convenient to use a special solver which accommodates this special topology. This will provide both speed of solution and efficient use of memory.
- Handling the span loading of the frame super element is currently not implemented. One has to convert the distributed span loading to a series of point loads and apply them through division joint super elements located along the span. This feature may be added to the frame super element.
- The frame super element is currently using a uniform mesh in which all frame elements and interface elements have the same size. A more sophisticated auto mesh generation or mesh update algorithm may be

added to increase the mesh density at critical parts of the super element to increase the accuracy without increasing the computational cost.

- Formulation of the joint super element may be extended to model larger size joints. This is necessary to keep the aspect ratio of the interface elements below a threshold value for such large joints.
- In the current formulation and implementation of the joint super element the anchorage conditions for the bolted corner pieces are handled either by changing the material parameters of the adhesive layer or assuming the interface and consequently the whole joint as completely rigid. This can be handled in a more sophisticated manner by reformulating the joint super element.
- The material module may be enhanced by adding a strain hardening parameter in order to implement the uniaxial plasticity. This will provide the damping or energy dissipation mechanism for axial deformations of the steel plates.
- A built-in material library which contains the commonly used concrete and steel classes might be implemented into the program.
- The moment-curvature module may be enhanced by adding a damage parameter in order to implement the actual plastic behavior of the beam. This will provide the damping or energy dissipation mechanism for bending deformations of the RC beam.
- The RC section moment-curvature generator may be added to the moment-curvature module to increase the integrity of the program.
- In addition to LU solver, other types of solvers such as iterative, symmetric, banded, sky-line solvers may be implemented.
- A special inversion algorithm may be developed for the condensation of the frame super element stiffness matrix. The new algorithm should take the special topology of the frame super element stiffness matrix into account.

REFERENCES

[1] R.D. Cook, D.S. Malkus and M.E. Plesha, "Concepts and Applications of Finite Element Analysis", John Wiley & Sons, 1989.

[2] K.J. Bathe, "Finite Element Procedures", Prentice-Hall, 1995.

[3] J.G. Teng, J.F. Chen, S.T. Smith and L. Lam, "FRP Strengthened RC Structures", John Wiley & Sons, 2001.

[4] E.E. Gdoutos, K. Pilakoutas and C.A. Rodopoulos, "Failure Analysis of Industrial Composite Materials", 2000.

[5] D. Duthinh and M. Starnes, "Strength and Ductility of Concrete Beams Reinforced with Carbon FRP and Steel" National Institute of Standards and Technology (2001)

[6] L. De Lorenzis, B. Miller and A. Nanni, "Bond of FRP Laminates to concrete", ACI Material Journal v.98 (2001) pp256-264

[7] A.J. Lamanna, L.C. Bank and D.W. Scott, "Flexural Strengthening of Reinforced Concrete Beams Using Fasteners and Fiber-Reinforced Polymer Strips ", ACI Structural Journal v.98 (2001) pp368-376

[8] J.F. Chen and J.G. Teng, "Anchorage Strength Models for FRP and Steel Plates Bonded to Concrete", Journal of Structural Engineering v.127 (2001) pp784-791

[9] S.T. Smith and J.G. Teng, "FRP-Strengthened RC Beams-I: Review of Debonding Strength Models", Engineering Structures v.24 (2002) pp385-395

[10] S.T. Smith and J.G. Teng, "FRP-Strengthened RC Beams-II: Assesment of Debonding Strength Models", Engineering Structures v.24 (2002) pp397-417

[11] Y. Qiu, M.A. Crisfield and G. Alfano, "An Interface Element Formulation for the Simulation of Delamination with Buckling", Engineering Fracture Mechanics v.68 (2001) pp1755-1776

[12] G. Li, P. Lee-Sullivan and R.W. Thring, "Nonlinear Finite Element Analysis of Stress and Strain Distributions across the Adhasive Thickness in Composite Single-Lap Joints", Composite Structures v.46 (1996) pp395-403

[13] P.C. Pandey and S. Narasimhan, "Three-Dimensional Nonlinear Analysis of Adhesively Bonded Lap Joints Considering Viscoplasticity in Adhesives", Computers and Structures v.79 (2001) pp769-783

[14] S.W. Hansen, "Strength Modeling and Analysis of Multilayer Laminated Plates" ESAIM: Proceedings v.4 (1998) pp117-135

[15] V. Colotti and G. Spadea, "Shear Strength of RC Beams Strengthened with Steel or FRP Plates" Journal of Structural Engineering v.127 (2001) pp367-373

[16] S.K. Kassegne and J.N. Reddy, "A Layerwise Shell Stiffener and Stand-Alone Curved Beam Element", Asian Journal of Structural Engineering, v.2 (1997) pp1-17

[17] R. Tanov and A. Tabiei, "Finite Element Implementation of a New Sandwich Homogenization Procedure", Composite Structures v.50 (2000) pp59-58

[18] S. Singh and I.K. Partridge, "Mixed-Mode Fracture in an Interleaved Carbon-Fibre/Epoxy Composite", Composites Science and Technology v.55 (1995) pp319-327

[19] H. Lou and S. Hanagud, "Dynamics of Delaminated Beams", International Journal of Solids and Structures v.37 (2000) pp1501-1519

[20] F. Shen, K.H. Lee and T.E.Tay, "Modeling Delamination Growth in Laminated Composites", Composites Science and Technology v.61 (2001) pp1239-1251

[21] N. El-Abbasi and S.A. Meguid, " A New Shell Element Accounting for Through-Thickness Deformation", Comput. Methods Appl. Mech. Engrg. v.189 (2000) pp841-862

[22] O.T. Thomsen, "High-Order Theory for the Analysis of Multi-Layer Plate Assemblies and Its Application for the Analysis of Sandwich Panels with Terminating Plies", Composite Structures v.50 (2000) pp227-238

[23] A. Aprile, E. Spacone and S. Limkatanyu, "Role of Bond in RC Beams Strengthened with Steel and FRP Plates", Journal of Structural Engineering v.127 (2000) pp1445-1452

[24] A. Aprile, S. Limkatanyu and E. Spacone, "Analysis of RC Beams Strengthened with FRP Plates", ASCE Structures Conference, Washington DC, (May 2001)

[25] M.J. Chajes, W.W. Finch, T.F. Januszka and T.A. Thomson, "Bond and Force Transfer of Composite Material Plates Bonded to Concrete", Journal of Structural Engineering v.127 (2000) pp1445-1452

[26] J.G. MacGregor, "Reinforced Concrete: Mechanics and Design", Englewood Cliffs, N.J.: Prentice Hall (1988)

[27] A. Habibullah and E.L. Wilson, "SAP2000 – Integrated Finite Element Analysis and Design of Structures", Computers and Structures Inc., (1997)

APPENDIX A

INPUT FILE FORMATS

The main program is composed of two modules which are the RC section moment-curvature generator module and the structural analysis module. The RC section moment-curvature generator module is run in order to prepare necessary moment-curvature relation data for the structural analysis module. The program asks the user which module to run at the beginning. Actually, execution of the program prints the following direction lines to screen.

```
[0] Analyze RC section to generate Moment-Curvature data
[1] Analyze RC frame structure
Input Analysis Option?
```

The user must enter "0" for the RC section moment-curvature generator and "1" for the structural analysis when the program asks "`Input Analysis Option?`".

Input file formats are kept as flexible as possible to write any explanatory comment about the data provided. In fact, it is possible to write these comments anywhere of the input file as long as the comment do not contain keywords and the "=" sign. There is, at least, one space before and after the "=" sign. Actually, each input data must immediately follow an "=" sign. The comments before "=" sign are optional and they are used only as explanatory purposes. The details of the input file format are explained below.

A.1 RC Section Moment-Curvature Generator Module

This module first asks for input file name. User must enter the full file name with its extension. Throughout the program, Newton (N) is used as a force unit, and millimeter (mm) is used as a length unit. Therefore, Input data must be compatible with these units, i.e., pressure unit must be MPa and moment unit must be N-mm, etc. A typical input file is given below.

```
Cover_Thickness_(mm)      =  15.0
Depth_of_Section_(mm)     = 150.0
Width_of_the_Section_(mm) = 120.0
Top_Steel_Area_(mm^2)     =  58.9
Bottom_Steel_Area_(mm^2)  = 235.6
Concrete_Compressive_Strength_(MPa) =     33.0
Rebar_Yield_Strength_(MPa)          =    384.0
Rebar_Elasticity_Modulus_(MPa)      = 200000.0
```

A.2 Structural Analysis Module

There are 7 different data blocks. Although the order of these data blocks is not important, to increase the readability of the input file, it should be in the order given in this text. A typical data block format is given below.

```
DATA-BLOCK
[keyword] = #
  [keyword] = #
  [keyword] = #
  ...
```

A.2.1 SYSYEM Data Block

SYSTEM identifier is used to define the global data of the structural system such as number of increments, convergence tolerance, convergence criteria to be used, output controls, etc. After the first "=" sign following the SYSTEM identifier, the number of load increments are given. After the second "=" sign, convergence tolerance is given. After the third "=" sign, number of maximum iterations is given. After the fourth, fifth and sixth "=" signs, displacement, force and energy convergence criteria controls are input, respectively. Seventh and eighth "=" signs are followed by joint and frame super elements' output controls. These control data is either "0" for "NO" or "1" for "YES".

```
SYSTEM
Number_of_Load_Increments     = 2
Convergence_Tolerance         = 0.01
Number_of_Maximum_Iterations  = 200
Use_Displacement_Convergence_Criteria = 1
Use_Force_Convergence_Criteria        = 1
Use_Energy_Convergence_Criteria       = 1
Print_JSE_Outputs_for_Each_Increment  = 1
Print_FSE_Outputs_for_Each_Increment  = 1
```

A.2.2 MATERIAL Data Block

MATERIAL identifier is used to define the material properties of the structural system. It contains the Poisson's ratio and piecewise linear stress-strain relation. After the first "=" sign following the MATERIAL identifier, the number of material types in the system must be given. For each material type, first "=" is for Poisson's ratio, following "=" sign stands for the number of stress-strain data points. Then, strains and stresses are given after next two "=" signs, respectively.

```
MATERIAL
Number_of_Materials = 3

MT0_Steel_or_FRP
  Poisson_Ratio = 0.3
  Number_of_Stress-Strain_Points = 2
    Strain = -1.735e-2  1.735e-2
    Stress = -3.140e+3  3.140e+3

MT1_Epoxy
  Poisson_Ratio = 0.2
  Number_of_Stress-Strain_Points = 2
    Strain = -1.563e-3  1.563e-3
    Stress = -2.000e+1  2.000e+1

MT2_Concrete
  Poisson_Ratio = 0.2
  Number_of_Stress-Strain_Points = 2
    Strain = -3.300e-3  3.300e-3
    Stress = -3.300e+1  3.300e+1
```

A.2.3 MOMENT-CURVATURE Data Block

MOMENT-CURVATURE identifier is used to define the piecewise linear moment-curvature relationship of frame elements in the structural system. After the first "=" sign following the MOMENT-CURVATURE identifier, the number of moment-

curvature relationships in the system are given. For moment-curvature relationship, first “=” sign stands for the number of moment-curvature data points. Then, curvatures and moments are given after next two “=” signs, respectively.

```
MOMENT-CURVATURE
Number_of_Moment-Curvatures = 2

MC0_RC_Beam
  Number_of_Moment-Curvature_Points = 4
  Curvature = -1.000e-3  -1.350e-5  3.911e-5  1.000e-3
  Moment    = -6.100e+6  -6.000e+6  1.700e+7  1.800e+7

MC1_steel_top_and_bottom_layer
  Number_of_Moment-Curvature_Points = 4
  Curvature = -2  -1  1  2
  Moment    = -1  -1  1  1
```

A.2.4 SECTION Data Block

SECTION identifier is used to define the section data of all the frame super elements in the structural system. For each section type, geometric dimensions, top and bottom strengthening interface and plate data, corresponding material data, etc. must be given. After the first “=” sign following the SECTION identifier, the number of sections in the system must be written. For each section, first “=” sign is followed by RC section area. Second “=” sign is followed by center to bottom and center to top distance, respectively. Third “=” sign is followed by bottom plate height and width, respectively. Fourth “=” sign is followed by top plate height and width, respectively. Fifth “=” sign is followed by bottom interface height and width, respectively. Sixth “=” sign is followed by top interface height and width, respectively. Seventh “=” sign is followed by middle, bottom and top layer material ids, respectively. Eighth “=” sign is followed by bottom and top interface material ids, respectively. Ninth “=” sign is followed by middle, bottom and top layer moment-curvature relation ids, respectively. Tenth “=” sign is followed by two control data for the existence of bottom and top strengthening plates, respectively.

```
SECTION
Number_of_Section = 1

SC0_Beam_Section
  RC_Section_Area = 18000.0
  Distance_of_Centerline_to_Bottom_and_Top = 75.0 75.0
  Bottom_Plate_Height-Width = 1.2 80.0
  Top_Plate_Height-Width    = 1.2 80.0
```

```
  Bottom_Interface_Height-Width = 4.0 80.0
  Top_Interface_Height-Width    = 4.0 80.0
  RC_and_Plate_MaterialIds_Middle-Bottom-Top = 2 0 0
  Interface_MaterialIds_Bottom-Top          = 1 1
  RC_and_Plate_Moment-CurvatureIds_Middle-Bottom-Top = 0 1 1
  Section_has_Bottom-Top_Plates = 0 0
```

A.2.5 BRACE-ELEMENT Data Block

BRACE-ELEMENT identifier is used to define the data of brace elements of the structural system. After the first "=" sign following the BRACE-ELEMENT identifier, the number of brace elements in the system are given. For each brace element, connectivity data and material properties must be written. In connectivity data B means bottom, T means top, L means left and R means right.

```
BRACE-ELEMENT
Number of Brace-Element-Data = 1

BE0
  Brace-Element_Connectivity_(BL-BR-TR-TL)   = 1  2  4  3
  Brace-Element_MaterialId                = 0
  Brace-Element_Moment-CurvatureId        = 0
```

A.2.6 JOINT-SUPER-ELEMENT Data Block

JOINT-SUPER-ELEMENT identifier is used to define the data of structural joints and master nodes of the structural system. After the first "=" sign following the JOINT-SUPER-ELEMENT identifier, the number of joint super elements in the system must be written. For each joint super element, position, applied force, restraint, corner piece size, interface layer and steel plate dimensions and properties are given.

```
JOINT-SUPER-ELEMENT
Number of Joint-Super-Element-Data = 4

JSE0
  Location_of_Joint-Super-Element      x1 x2    = 0.0  0.0
  Applied_Force_to_Joint-Super-Element f1 f2 f3 = 0.0  0.0  0.0
  Restraints_of_Joint-Super-Element    r1 r2 r3 = 1    1    0
  Corner_Piece_Size              = 0.0
  Interface_Thickness_and_Width  = 4.0  80.0
  Plate_Thickness_and_Width      = 1.2  80.0
  Interface_and_Plate_MaterialId = 1 2
  Plate_Moment-CurvatureId       = 1
  Is_Joint-Super-Element_Rigid?  = 1
```

```
JSE1
  Location_of_Joint-Super-Element      x1 x2    = 10.0  0.0
  Applied_Force_to_Joint-Super-Element f1 f2 f3 =  0.0  0.0  0.0
  Restraints_of_Joint-Super-Element    r1 r2 r3 =  0    0    0
  Corner_Piece_Size              = 0.0
  Interface_Thickness_and_Width  = 4.0  80.0
  Plate_Thickness_and_Width      = 1.2  80.0
  Interface_and_Plate_MaterialId = 1 2
  Plate_Moment-CurvatureId       = 1
  Is_Joint-Super-Element_Rigid?  = 0
```

A.2.7 FRAME-SUPER-ELEMENT Data Block

`FRAME-SUPER-ELEMENT` identifier is used to define the frame element data of the structural system. After the first "=" sign following the `FRAME-SUPER-ELEMENT` identifier, the number of frame super elements in the system must be given. For each super element, connectivity, section data, and number of divisions that the element is to be divided must be given.

```
FRAME-SUPER-ELEMENT
Number_of_Frame-Super-Element = 3

FSE0
  Start_Joint-Super-ElementId = 0
  End_Joint-Super-ElementId   = 1
  SectionId                   = 0
  Number_of_Divisions         = 4
```

There are some important rules in defining the frame super element. If one does not obey these, rules the program will terminate and form an `err.txt` file, which explains the reason for the termination.

A.2.8 Possible Error Messages

Possible error messages which may be printed to a file named as "err.txt" are explained here with their reasons.

`ERROR: maxAspectRatio is exceeded`

As explain before in chapter 2, there are some limitations on interface element. Interface element maximum aspect ratio is set as 100.0 in the program. If this value is exceeded, user must reduce it by increasing number of divisions of frame

super element, by increasing interface element thickness, or by using more super elements.

ERROR: FSE is oblique

There are also some limitations on frame super elements. The program performs the analysis of orthogonal frame structures only. Unless all the frame super elements are horizontal or vertical, “Error: FSE is oblique” error message will be printed to “err.txt” file. Incase this error message is printed even if all the frame super elements are horizontal or vertical, the connectivity of the super element must be corrected. The program allows frame super element connectivity either from left to right or from bottom to top.

ERROR: Maximum Number of Divisions Exceeded

Number of divisions of frame macro element determines directly number of slave DOFs, and number of frame and interface elements which compose the super element. Very large number of divisions will adversely affect the efficiency and may cause memory problems. Because of this reasons, number of divisions is limited. The user should use more super elements instead of increasing the number of divisions.

ERROR: JSE type conflict

There are mainly three types of joint super elements fully rigid, flexible, and division joint super elements. These types are decided according to connectivity and joint super element input data. If there is a conflict in the connectivity or data i.e., the program can not assign the convenient type to the joint, this error message is printed to the “err.txt” file.

ERROR: Beam sections conflict

ERROR: Column sections conflict

A joint super element may connect two horizontal or vertical frame super elements. Formulation of the super element requires that the RC section dimensions of these two horizontal or vertical frame super elements must be the same. If they are not the same, program will print the convenient error message to the “err.txt” file.

ERROR: JSE does not connected to any FSE

As the message implies, a joint super element in the system is not connect to any frame super element. Program does not permit such a situation prints the error message to the “err.txt” file.

`ERROR: Incompatible Matrix Size`

Program uses an LU solver for the solution of linear equation system. If somehow there is an incompatibility in matrix sizes, i.e., matrix size may be zero or greater than maximum allowed size, the error message is printed to the “err.txt” file.

`ERROR: Maximum Number of JSEDs Exceeded`
`ERROR: Maximum Number of FSEDs Exceeded`
`ERROR: Maximum Number of BEDs Exceeded`
`ERROR: Maximum Number of MCs Exceeded`
`ERROR: Maximum Number of SCs Exceeded`
`ERROR: Maximum Number of MTs Exceeded`

All of the above error messages are related with the size limitations in the program. These size limitations are put in order not to cause any memory problems for large systems. For most of the structure, current limits are adequate. Incase one requires more capacity, the limits in the program source code must be modified and the executable file must be re-compiled.

APPENDIX B

RC SECTION MOMENT-CURVATURE GENERATOR

Main program, which is the structural analysis module, takes moment-curvature data as input. Therefore, user may obtain moment-curvature data by using other programs or methods. Also, the developed program gives an opportunity module for the generation of approximate moment-curvature relation for single or double reinforced rectangular unconfined sections. A typical double reinforced RC section is shown in Figure B.1.

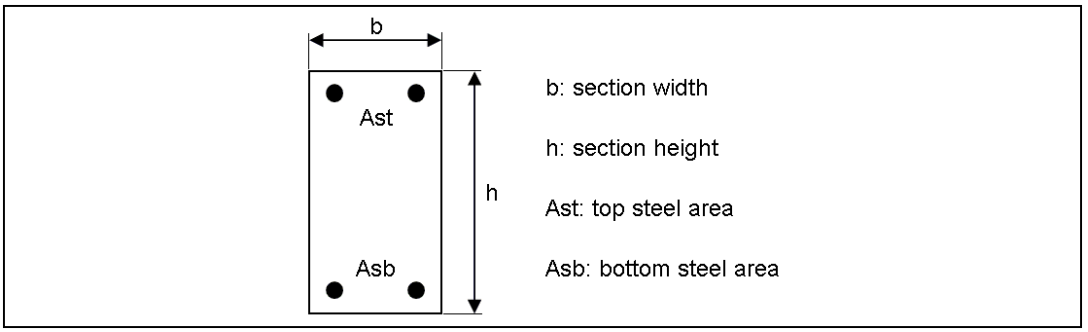

Figure B.1 A typical double reinforced RC section

For the sake of simplicity, the moments at three levels of curvature are established, i.e., a tri-linear moment-curvature relation is generated. These points are (M_{cr},ϕ_{cr}) which is symmetric for positive and negative moments, (M_y,ϕ_y) and (M_u,ϕ_u) which are calculated for positive and negative moments separately. A typical generated tri-linear moment-curvature diagram is shown in Figure B.2.

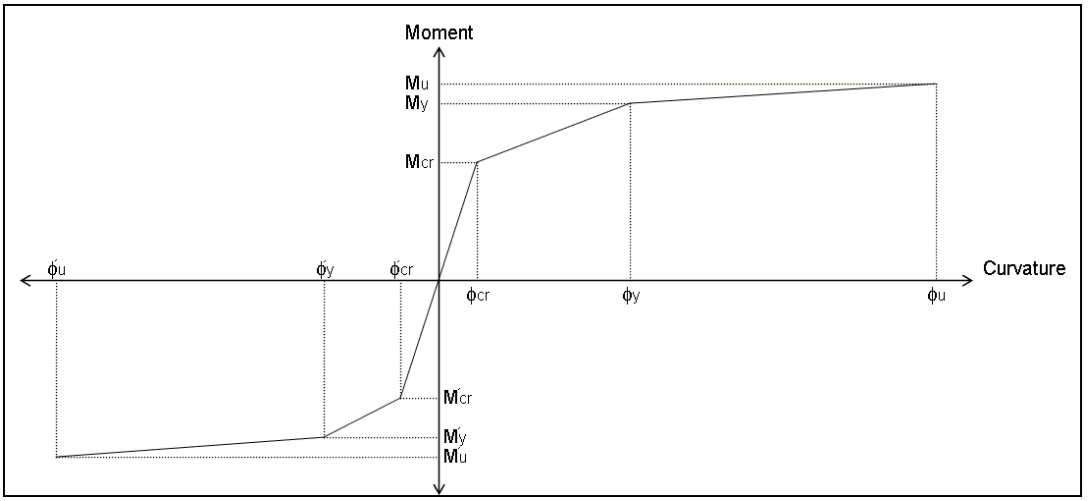

Figure B.2 Tri-linear moment-curvature diagram

This analysis represents the simplest of all moment-curvature analyses. Some simplifying assumptions are made to calculate the moment-curvature (M,ϕ) relationships, and all of these assumptions are basic the assumptions in flexural theory, namely,

1. Sections perpendicular to the axis of bending that are plane before bending are plane after bending, or plane sections remain plane. See Figure B.3.
2. The strain in the rebar is equal to the strain in the concrete at the same level in the cross section.
3. The stresses in the steel and concrete can be established from the individual stress-strain relationships.
4. In the calculations, compression steel is ignored for the sake of simplicity because although it complicates the computations a lot, its effect on the results are negligibly small.

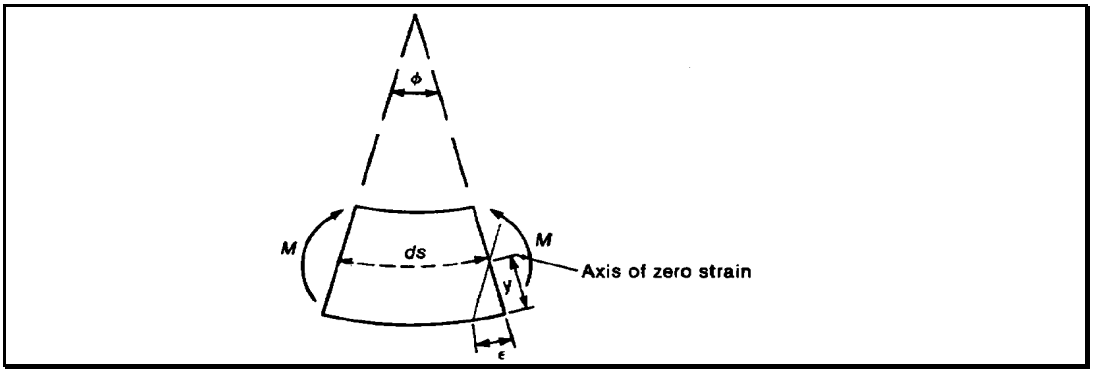

Figure B.3 Plane sections remain plane

As such, curvature and strains are related as given in Equation B.1. In this equation ε is the bottom fiber strain and y is the distance from the neutral axis.

$$\phi = \frac{\varepsilon}{y} \qquad (B.1)$$

B.1 Cracking Moment (M_{cr})

Cracking moment M_{cr} and corresponding cracking curvature ϕ_{cr} can be obtained by using Equation B.2. [26]. In these expressions, y_t is the distance from centroid to extreme tension fiber, f_r is the modulus of rupture, I_g is moment of inertia of the concrete section and E_c is modulus of elasticity of concrete.

$$M_{cr} = \frac{f_r \cdot I_g}{y_t}$$
$$\phi_{cr} = \frac{M_{cr}}{E_c \cdot I_g} \qquad (B.2)$$

Modulus of elasticity E_c and modulus of rupture f_r of concrete and moment of inertia I_g of concrete section are given in Equation B.3. In these equation f_c are the concrete compressive strength and its unit must be MPa and b is section width and h is section height.

$$E_c = 3250\sqrt{f_c} + 14000$$
$$f_r = 0.623\sqrt{f_c} \qquad (B.3)$$
$$I_g = \frac{1}{12} \cdot b \cdot h^3$$

B.2 Yield Moment (M_y)

Up to yielding, the beam is assumed to behave elastically. For computations, transferred section is used. This is performed by replacing area of tension steel (compression steel is ignored) with an area of concrete having the same axial stiffness EA. Transformed section and assumed stress distribution are shown in Figure B.4.

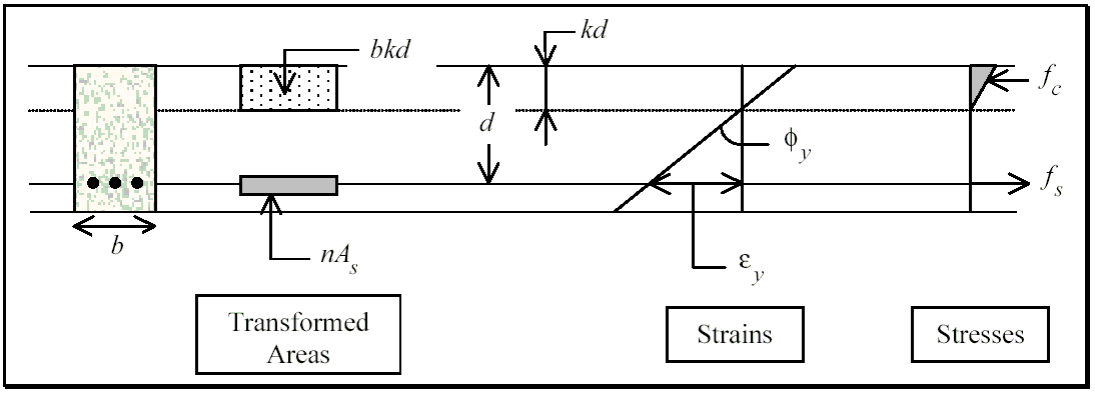

Figure B.4 Transformed section and assumed stress distribution in the concrete

The depth to the neutral axis is kd. The strain in the rebar is yield strain ε_y. For a singly reinforced section, k factor is given in Equation B.4. [26].

$$n = \frac{E_s}{E_c}$$
$$\rho = \frac{A_s}{b \cdot d} \qquad (B.4)$$
$$k = \sqrt{\rho \cdot n \cdot (2 + \rho \cdot n)} - \rho \cdot n$$

Yield moment M_y can be obtained by taking moments about the centroid of the concrete compression block, which is located at a distance of kd/3 below the top of the section. Expressions for yield moment M_y and corresponding curvature ϕ_y are given in Equation B.5.

$$M_y = A_s \cdot f_y \cdot \left(d - \frac{k \cdot d}{3} \right) \qquad (B.5)$$
$$\phi_y = \frac{\varepsilon_y}{d - k \cdot d}$$

B.3 Ultimate Moment Capacity (M_u)

Rectangular (Whitney-type) stress block is assumed in order to calculate the depth to the neutral axis c. Assumed rectangular stress block is shown in Figure B.5. Maximum compressive strain $\varepsilon_{c\,max}$ and β_1 factor are taken as 0.003 and 0.85 for normal strength concrete, respectively.

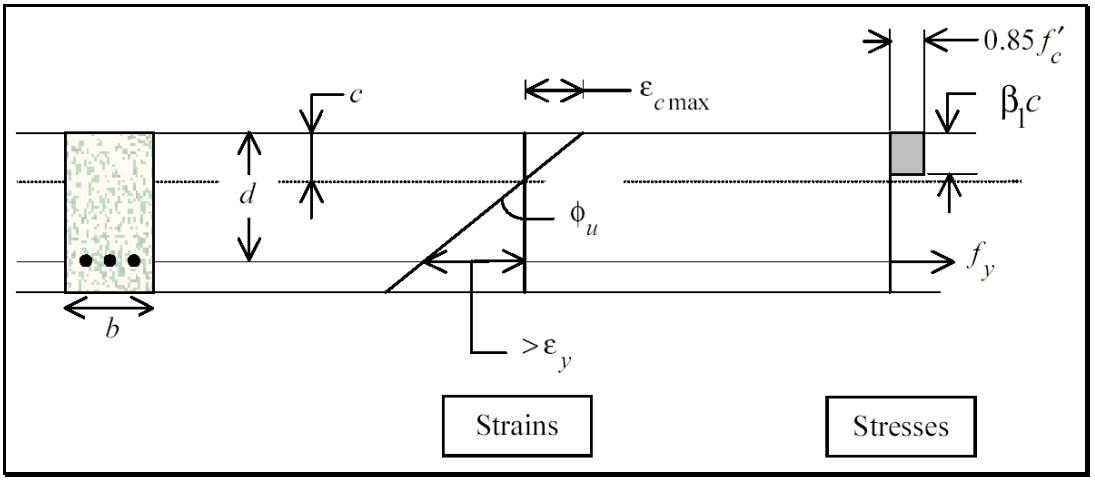

Figure B.5 Assumed stress distribution in the concrete

The ultimate moment capacity M_u is calculated in the traditional manner. Expressions for ultimate moment capacity M_u and corresponding curvature ϕ_u are given in Equation B.6.

$$M_u = A_s \cdot f_y \cdot \left(d - \frac{\beta_1 \cdot c}{2} \right)$$

$$\phi_u = \frac{\varepsilon_{c\,max}}{c} \qquad \text{(B.6)}$$